



Choi, S. et al. (2020) Parallel ascending spinal pathways for affective touch and pain. *Nature*, 587, pp. 258-263. (doi: [10.1038/s41586-020-2860-1](https://doi.org/10.1038/s41586-020-2860-1))

The material cannot be used for any other purpose without further permission of the publisher and is for private use only.

There may be differences between this version and the published version. You are advised to consult the publisher's version if you wish to cite from it.

<http://eprints.gla.ac.uk/226065/>

Deposited on 10 November 2020

Enlighten – Research publications by members of the University of
Glasgow

<http://eprints.gla.ac.uk>

1
2
3
4
5
6
7
8
9
10
11
12
13
14
15
16
17
18
19
20
21
22
23
24
25
26
27
28
29
30
31
32
33

Parallel ascending spinal pathways for affective touch and pain

Seungwon Choi¹, Junichi Hachisuka^{2,5}, Matthew A. Brett¹, Alexandra Magee¹, Yu Omori^{2,6},
Noor-ul-Aine Iqbal¹, Dawei Zhang¹, Michelle M. DeLisle¹, Rachel L. Wolfson¹, Ling Bai¹,
Celine Santiago¹, Shiaoqing Gong³, Martyn Goulding⁴, Nathaniel Heintz³, H. Richard Koerber²,
Sarah E. Ross², and David D. Ginty^{1*}

¹Department of Neurobiology, Howard Hughes Medical Institute, Harvard Medical School, 220
Longwood Avenue, Boston, MA 02115, USA

²Department of Neurobiology and the Pittsburgh Center for Pain Research, University of
Pittsburgh, Pittsburgh, PA 15213, USA

³The Laboratory of Molecular Biology, Howard Hughes Medical Institute, The Rockefeller
University, New York, NY 10065, USA

⁴Molecular Neurobiology Laboratory, The Salk Institute for Biological Studies, 10010 North
Torrey Pines Road, La Jolla, CA 92037, USA

⁵Current address: Institute of Neuroscience and Psychology, Sir James Black Building,
University of Glasgow, University Avenue, Glasgow G12 8QQ, United Kingdom

⁶Current address: Toray Industries, Inc., Pharmaceutical Research Laboratories,
10-1, Teburo 6-chome, Kamakura, Kanagawa 248-8555, Japan.

*correspondence: david_ginty@hms.harvard.edu

34 **Summary**

35 The anterolateral pathway consists of ascending spinal tracts that convey pain, temperature and
36 touch information from the spinal cord to the brain¹⁻⁴. Projection neurons (PNs) of the
37 anterolateral pathway are attractive therapeutic targets for pain treatment because nociceptive
38 signals emanating from the periphery channel through these spinal PNs *en route* to the brain.
39 However, the organizational logic of the anterolateral pathway remains elusive. Here, we show
40 that two PN populations that express structurally related GPCRs, TACR1 and GPR83, form
41 parallel ascending circuit modules that cooperate to convey tactile, thermal and noxious
42 cutaneous signals from the spinal cord to the lateral parabrachial nucleus of the pons (PBN_L).
43 Axons of *Tacr1*- and *Gpr83*-expressing spinoparabrachial (SPB) neurons innervate distinct sets
44 of PBN_L subnuclei, and strong optogenetic stimulation of their axon terminals induces distinct
45 escape behaviors and autonomic responses. Moreover, *Gpr83*-expressing SPB neurons are highly
46 sensitive to cutaneous mechanical stimuli and receive strong synaptic inputs from both high- and
47 low-threshold primary mechanosensory neurons. Remarkably, the valence associated with
48 activation of *Gpr83*-expressing SPB neurons is either positive or negative depending on stimulus
49 intensity. These findings reveal anatomically, physiologically, and functionally distinct SPB tract
50 subdivisions that underlie affective aspects of touch and pain.

51 While primary sensory neurons that respond to a range of innocuous or noxious stimuli acting on
52 the skin have been identified and characterized^{1,2,5}, less is known about how their signals are
53 integrated and processed within the spinal cord and conveyed via spinal PNs to the brain to
54 underlie somatosensory perception and behavior. Here, we sought to generate mouse genetic
55 tools for spinal cord anterolateral pathway PNs and use them for anatomical,
56 electrophysiological, and behavioral analyses to define ascending pathways that underlie
57 affective touch and pain.

58

59 **Genetically defined spinal PN subsets**

60 We generated a *Tacr1^{CreERT2}* knockin mouse line (Fig. 1a, Extended Data Fig. 1a2, b1-3) and
61 found that *Tacr1⁺* SPB neurons are *Gad2*-negative and represent a large subset ($57.3 \pm 4.7\%$) of
62 the total SPB population (Extended Data Fig. 2a, b, e, f), as previously reported^{3,6}. In addition, to
63 identify other, novel subsets of SPB neurons, we conducted an *in silico* screen of BAC-GFP
64 transgenic mouse lines from the GENSAT project⁷. One of these lines, *Gpr83-GFP*, was found
65 to label a major subset of SPB neurons ($52.7 \pm 4.4\%$ of the total SPB population) (Fig. 1b). In
66 addition, a newly generated *Gpr83^{CreERT2}* knockin mouse line labels PNs of the anterolateral
67 pathway that are *Gad2*-negative and account for $45.2 \pm 2.4\%$ of SPB neurons (Extended Data
68 Fig. 1a3, c, 2a, b, e, f). Further analysis revealed that the *Gpr83⁺* and *Tacr1⁺* SPB populations are
69 numerically comparable, largely non-overlapping, and together account for the majority ($88.4 \pm$
70 2.7%) of SPB neurons in spinal cord lamina I+IIo (Fig. 1f-h, Extended Data Fig. 2e-g). *Tacr1⁺*
71 SPB neurons, a previously reported SPB populations⁸, account for $22.1 \pm 3.4\%$ of SPB neurons
72 in lamina I+IIo, and *Tacr1* is expressed in subsets of both *Tacr1⁺* and *Gpr83⁺* SPB neurons (38.2
73 $\pm 4.0\%$ and $47.8 \pm 9.7\%$, respectively), suggesting that *Tacr1⁺* SPB neurons may represent the
74 small subset of SPB neurons that express both *Tacr1* and *Gpr83* (Extended Data Fig. 2j-n). We
75 also generated a *Robo3^{ires-CreERT2}* knockin mouse line (Extended Data Fig. 1a1) because *Robo3*
76 is transiently expressed in developing commissural neurons⁹, including PNs of the anterolateral
77 pathway.

78

79 To define brain targets of anterolateral pathway PNs, we visualized axonal projections of
80 *Tacr1⁺*, *Gpr83⁺*, or *Robo3⁺* spinal PNs to the brain using intersectional genetic strategies (PN
81 Cre; *Lbx1^{FlpO10}* (or *Cdx2-NSE-FlpO11*); *Rosa26^{FSF-LSL-tdTomato}*). We observed that the PBN_L is the

82 most densely innervated brain region for both *Tacr1*⁺ and *Gpr83*⁺ spinal PNs (Fig. 1c, d, e). In
83 the thalamus, medial and posterior thalamic nuclei are innervated by both *Tacr1*⁺ and *Gpr83*⁺
84 spinal PNs in a partially overlapping manner (Fig. 1c, d). In contrast, the ventral posterolateral
85 nucleus of the thalamus (VPL) is innervated by *Robo3*⁺ spinal PNs (Extended Data Fig. 1d). In
86 the midbrain, both *Tacr1*⁺ and *Gpr83*⁺ spinal PNs innervate the lateral region of the
87 periaqueductal grey (PAG) and the midbrain reticular nucleus (MRN), while *Tacr1*⁺ spinal PNs
88 more densely innervate the superior colliculus with a compartmentalized array of terminal
89 patches in the intermediate grey layer (SCig) (Fig. 1c, d). In the brainstem, both *Tacr1*⁺ and
90 *Gpr83*⁺ PNs innervate the medial accessory olive (MAO) and the lateral reticular nucleus (LRN),
91 while *Gpr83*⁺ PNs uniquely innervate the dorsal fold of the dorsal accessory olive (DAOdf)
92 (Extended Data Fig. 2h, i). Anatomical analyses using a dual-virus labeling approach (Extended
93 Data Fig. 3) revealed that axons of both *Tacr1*⁺ and *Gpr83*⁺ posterior thalamus-projecting
94 neurons travel through the ventral lateral funiculus of the spinal cord white matter and form
95 collateral branches that terminate in the MAO and LRN of the ventral brainstem. In contrast,
96 axons of *Tacr1*⁺ SCig-projecting neurons travel through the dorsal lateral funiculus and form
97 collateral branches that terminate in the PAG. Strikingly, none of these thalamic- and midbrain-
98 projecting *Tacr1*⁺ or *Gpr83*⁺ PNs formed collateral branches terminating within the PBN_L, the
99 most densely innervated brain target of anterolateral pathway PNs. These findings indicate that
100 *Tacr1*⁺ and *Gpr83*⁺ spinal PNs that innervate the posterior thalamus, midbrain, and PBN_L are
101 distinct populations.

102

103 **Zonal segregation of SPB axon terminals**

104 The PBN_L is comprised of several cytoarchitecturally distinct subnuclei that have distinct
105 input/output connections with other brain regions^{12,13}. We found that the axons of spinal PNs,
106 labeled in their entirety using *Cdx2-Cre; Rosa26^{LSL}-synaptophysin-tdTomato* mice, terminate within all
107 PBN_L subnuclei, except for the ventrolateral subnucleus (PBN_{VL}) and the center region of the
108 external lateral subnucleus (PBN_{EL}) (Fig. 2a). Whereas *Tacr1*⁺ SPB neurons form synapses
109 mainly within the central lateral (PBN_{CL}) and internal lateral (PBN_{IL}) subnuclei, *Gpr83*⁺ SPB
110 neurons form synapses uniquely within the dorsal lateral (PBN_{DL}) and PBN_{EL} subnuclei, in
111 addition to the PBN_{IL} (Fig. 2b, c, d). Accordingly, presynaptic terminals of *Gpr83*⁺ SPB neurons
112 are associated with CGRP⁺ neurons within the PBN_{EL}¹⁴, whereas *Tacr1*⁺ axon terminals are not

113 (Extended Data Fig. 4a, b). Moreover, *Tacr1*⁺ SPB neurons form synapses only within the PBN_{IL}.
114 (Extended Data Fig. 2o-q), which is the sole PBN_L subnucleus receiving both *Tacr1*⁺ and *Gpr83*⁺
115 SPB synaptic terminals (Fig. 2c, d). Thus, distinct SPB populations form synaptic terminals
116 within the PBN_L in a zonally segregated manner.

117

118 The finding that *Tacr1*⁺ and *Gpr83*⁺ SPB neurons innervate distinct sets of PBN_L
119 subnuclei led us to hypothesize that these two SPB populations underlie distinct behavioral
120 responses to somatosensory stimuli. Selective, bilateral optogenetic activation of either *Tacr1*⁺ or
121 *Gpr83*⁺ SPB neuron axon terminals within the PBN_L (Fig. 2e) strongly induced the expression of
122 the immediate early gene Fos in the respective PBN_L subnuclei (Fig. 2f, g) predicted by the
123 synaptic terminal analysis (Fig. 2b, c, d). Interestingly, strong stimulation of *Tacr1*⁺ axon
124 terminals also resulted in Fos expression in the PBN_{EL}, in addition to the PBN_{CL} and PBN_{IL} (Fig.
125 2f, g), consistent with the presence of local microcircuits that interconnect these PBN_L
126 subnuclei¹⁵. Behaviorally, high-power (6.5 mW) optogenetic stimulation of either *Tacr1*⁺ or
127 *Gpr83*⁺ SPB neuron terminals led to a robust increase in locomotion in a time-locked manner
128 (Fig. 2h, i), reminiscent of escape behaviors observed in response to noxious stimuli.
129 Interestingly, while *Gpr83*⁺ terminal stimulation promoted forward locomotion, *Tacr1*⁺ terminal
130 stimulation induced a pronounced backward “retreat” behavior as well as jumping (Fig. 2j,
131 Extended Data Fig. 4d-f, Supplementary Video 1-3). Both light-activated hyperlocomotion and
132 jumping were abolished following infusion of the glutamatergic synaptic blocker NBQX into the
133 PBN_L (Fig. 2k, l), and Fos induction was not observed in the spinal cord following
134 photostimulation of SPB axon terminals (Extended Data Fig. 4g, h), suggesting that escape
135 behaviors evoked by SPB axon terminal stimulation is mediated by glutamatergic synaptic
136 transmission within the PBN_L and not by backpropagating action potentials and activation of
137 other brain regions or the spinal cord. It is noteworthy that light-evoked increases in locomotion
138 were followed by a robust “freezing” behavior that lasted for the entire light-off period
139 (Extended Data Fig. 4c, Supplementary Video 4). Moreover, activation of either *Tacr1*⁺ or
140 *Gpr83*⁺ SPB neurons led to an increase in pupil diameter (Fig. 2m, n), which likely reflects
141 increased sympathetic tone. While pupillary dilation evoked by *Gpr83*⁺ SPB terminal stimulation
142 was transient (fast decay and small area under curve), dilation evoked by *Tacr1*⁺ SPB terminal
143 stimulation was sustained (Fig. 2m, o). *Tacr1*⁺ SPB terminal stimulation additionally induced

144 squinting/blinking, indicative of severe pain¹⁶ (Fig. 2m, p). These findings suggest that high-
145 intensity stimulation of *Tacr1*⁺ and *Gpr83*⁺ SPB neurons induces nocifensive behaviors, but
146 these two SPB populations differentially influence the mode of escape locomotor behavior and
147 the temporal dynamics of autonomic responses.

148

149 **A mechanosensory limb of the SPB pathway**

150 PNs of the anterolateral pathway are heterogeneous in terms of their physiological response
151 properties, and the majority are polymodal^{3,17-20}. To determine the response properties of *Gpr83*⁺
152 and *Tacr1*⁺ SPB subsets, we conducted whole-cell patch-clamp recordings from these two
153 neuronal populations using an *ex vivo* skin-spinal cord preparation¹⁸ (Fig. 3a). Despite
154 heterogeneity in the tuning properties among individual *Gpr83*⁺ and *Tacr1*⁺ SPB neurons,
155 *Gpr83*⁺ and *Tacr1*⁺ SPB subsets at the population level exhibited distinct responses to
156 mechanical and thermal stimuli (Fig. 3b-g, Extended Data Fig. 5a, b); *Gpr83*⁺ SPB neurons were
157 highly sensitive to mechanical stimuli (Fig. 3e), whereas *Tacr1*⁺ SPB neurons were more
158 responsive to innocuous thermal stimuli, cool temperature (15°C) in particular, and capsaicin
159 than *Gpr83*⁺ SPB neurons (Fig. 3f, Extended Data Fig. 5c, d). Interestingly, *Gpr83*⁺ and *Tacr1*⁺
160 SPB neurons both responded to noxious cold (0°C) and noxious heat (54°C) (Fig. 3g),
161 suggesting that both of these SPB subdivisions convey noxious thermal signals.

162

163 Consistent with these *ex vivo* recordings, extensive paw-licking, a nocifensive behavior,
164 elicited by noxious heat (55°C) or noxious cold (5°C) and reactivity to noxious mechanical
165 stimuli as well as rough floor aversion were diminished when neurotransmission was suppressed
166 in both *Gpr83*⁺ and *Tacr1*⁺ spinal neurons, including SPB neurons, simultaneously but not when
167 neurotransmission was suppressed in either *Gpr83*⁺ or *Tacr1*⁺ spinal neurons alone (Extended
168 Data Fig. 6). Together, these physiological and behavioral findings suggest that *Gpr83*⁺ and
169 *Tacr1*⁺ SPB populations differentially transmit innocuous cutaneous signals to the brain, while
170 noxious tactile and thermal signals are conveyed by both SPB subdivisions.

171

172 To define spinal cord circuit mechanisms that account for differences in stimulus-
173 response properties of *Tacr1*⁺ and *Gpr83*⁺ SPB neurons, we next examined the sensory neuron
174 inputs onto these SPB neurons using channelrhodopsin-assisted circuit mapping in acute spinal

175 cord slices (Fig. 3h). Photostimulation (473 nm) of CGRP⁺ peptidergic nociceptor terminals,
176 labeled using a newly generated BAC transgenic mouse line, *Calca-FlpE* (Extended Data Fig.
177 1f), evoked large EPSCs and action potential firing in most *Tacr1*⁺ SPB neurons, but not in
178 *Gpr83*⁺ SPB neurons (Fig. 3j, k) except for a small fraction that exhibited small polysynaptic
179 EPSCs evoked with much longer light pulses (Extended Data Fig. 7b). In contrast, activation of
180 either *Mrgprb4*⁺ mechanosensory neuron²¹ terminals or *Ntrk2*⁺ (also known as *TrkB*) A δ -low
181 threshold mechanoreceptor (LTMR)²² terminals evoked large EPSCs and action potential firing
182 in the majority of *Gpr83*⁺ SPB neurons, but not in *Tacr1*⁺ SPB neurons (Fig. 3l-o) except for a
183 small fraction that exhibited small polysynaptic EPSCs evoked with much longer light pulses
184 (Extended Data Fig. 7c, d). Activation of *Mrgprd*⁺ polymodal non-peptidergic sensory neuron²³
185 terminals evoked large EPSCs and action potential firing in both *Gpr83*⁺ and *Tacr1*⁺ SPB
186 neurons (Extended Data Fig. 7e, f). A morphological correlate of the differential sensory neuron
187 inputs is that dendrites of *Tacr1*⁺ SPB neurons are restricted to the most superficial spinal cord
188 lamina, where most CGRP⁺ peptidergic nociceptors terminate, whereas dendrites of *Gpr83*⁺ SPB
189 neurons often extend into lamina II_{id}, the site of non-peptidergic sensory neuron synapses,
190 including those of *Mrgprb4*⁺ mechanosensory neurons, and even into lamina II_{iv} and III, the site
191 of A δ -LTMR and A β -LTMR synapses (Extended Data Fig. 7g-k). Thus, the distinct
192 physiological responses of *Gpr83*⁺ and *Tacr1*⁺ SPB neurons to tactile and thermal stimuli can be
193 explained by differences in their dendritic morphologies and synaptic inputs from distinct classes
194 of mechanosensory neurons and nociceptors.

195

196 **SPB neuronal subsets and hedonic value**

197 Several lines of evidence indicate that the organizational properties of the *Gpr83*⁺ and *Tacr1*⁺
198 SPB subdivisions are distinct from other ascending pathways of anterolateral spinal tracts. First,
199 in contrast to other brain targets, including the PAG and SC_{ig}, which are innervated by axons
200 originating exclusively from the contralateral side of the spinal cord, the PBN_L was found to
201 receive bilateral input from both *Gpr83*⁺ and *Tacr1*⁺ SPB neurons (Fig. 4a, b). Simultaneous
202 retrograde tracing of SPB neurons innervating either side of the PBN_L (Extended Data Fig. 8a-c)
203 and anterograde tracing of sparsely labeled SPB axons (Fig. 4c-f) revealed that individual SPB
204 neurons project either contralaterally, ipsilaterally, or bilaterally. Second, consistent with our
205 observations from dual-virus retrograde labeling experiments (Extended Data Fig. 3), single

206 axon tracing analyses of sparsely labeled *Gpr83*⁺ and *Tacr1*⁺ SPB neurons support the idea that
207 most SPB neurons are dedicated anterolateral pathway PNs that innervate the PBN_L without
208 forming collateral branches that innervate other brain regions (Fig. 4e). In contrast, anterolateral
209 pathway PNs with axons innervating the inferior olivary complex have collateral branches that
210 extend to other brain regions (Extended Data Fig. 3f, i, 8d, e). Third, unlike other brain targets of
211 the anterolateral pathway, such as the inferior olivary complex (Extended Data Fig. 8f), we
212 observed no somatotopic organization of SPB axon terminals within the PBN_L (Fig. 4g-i).

213

214 These unique anatomical features led us to suspect that the *Tacr1*⁺ and *Gpr83*⁺ SPB
215 subdivisions contribute to affective, rather than discriminative aspects of somatosensation.
216 Consistent with this idea, activation of SPB neurons with moderate-intensity stimulation (1 mW),
217 particularly *Tacr1*⁺ SPB neurons, induced robust, repetitive grooming of forepaw and head
218 (Extended Data Fig. 9a, b, Supplementary Video 5), which in rodents is a hallmark feature of
219 stress and anxiety²⁴. Selective activation of SPB axon terminals originating exclusively from the
220 lumbar spinal cord also induced this rostral grooming behavior, but not grooming of body trunk,
221 hindpaw, or tail (Extended Data Fig. 9c, d), consistent with the idea that the SPB pathways lack
222 somatotopic organization. Moreover, high-intensity photostimulation (6.5 mW) of either *Tacr1*⁺
223 or *Gpr83*⁺ SPB axon terminals within the PBN_L induced strong place aversion (Fig. 5a, b).
224 Interestingly, the aversive effect of high-intensity photostimulation of *Gpr83*⁺ SPB neurons was
225 transient and lasted only for the stimulation period, whereas activation of *Tacr1*⁺ SPB neurons
226 led to a sustained aversive behavior that continued after the stimulation period had ended,
227 suggesting that strong activation of SPB neurons, particularly *Tacr1*⁺ SPB neurons, evokes
228 behaviors associated with negative emotional valence.

229

230 In addition to negative valence associated with noxious stimuli, observations in human
231 patients with anterolateral cordotomy have implicated the anterolateral pathway in conveying
232 signals associated with positive valence and pleasurable properties of gentle touch²⁵⁻²⁷. Our
233 finding that *Gpr83*⁺ SPB neurons are much more responsive than *Tacr1*⁺ SPB neurons to light
234 mechanical forces acting on the skin and receive strong synaptic inputs from mechanosensory
235 neurons, including LTMRs, prompted us to ask whether *Gpr83*⁺ SPB neurons convey signals
236 that underlie positive valence associated with light touch as well as negative valence associated

237 with noxious stimuli. To address this, we developed an optogenetic stimulation-coupled
238 instrumental conditioning assay in which mice receive selective optogenetic stimulation of either
239 *Tacr1*⁺ or *Gpr83*⁺ SPB axon terminals in the PBN_L upon pressing an active lever, but not an
240 inactive lever (Fig. 5d). Remarkably, low-intensity, self-administered photostimulation (0.4 mW)
241 of *Gpr83*⁺ SPB neurons, but not *Tacr1*⁺ SPB neurons, promoted positive reinforcement (i.e.
242 increased lever-pressing) over time, whereas moderate-intensity photostimulation (1 mW) of
243 either *Tacr1*⁺ or *Gpr83*⁺ SPB neurons served as a punishment signal (i.e. decreased lever-
244 pressing) (Fig. 5e, f, Extended Data Fig. 9e, f). Interestingly, elevated lever-pressing and positive
245 reinforcement associated with weak optogenetic stimulation of *Gpr83*⁺ SPB neurons was
246 observed for several days after photostimulation was uncoupled from pressing the active lever.
247 Similarly, in a real-time place preference paradigm, only *Gpr83*^{CreERT2}; *Lbx1*^{FlpO}; *Rosa26*^{LSL-FSF-}
248 *ReaChR* mice exhibited preference for the stimulated side of the chamber following the period of
249 moderate-intensity photostimulation (1 mW), but not strong photostimulation (6.5 mW) (Fig. 5b,
250 c).

251
252 To begin to define cellular and circuit level correlates of intensity-dependent changes in
253 behaviors associated with different valences (positive or negative), we next examined Fos
254 induction in the PBN_L following photostimulation of SPB axon terminals with different optical
255 strengths. High-intensity photostimulation (6.5 mW) of *Gpr83*⁺ SPB axons terminals resulted in
256 strong Fos induction in all three PBN_L subnuclei in which *Gpr83*⁺ SPB axons terminals are
257 associated, whereas low-intensity photostimulation (0.4 mW) induced Fos expression only in the
258 PBN_{EL} (Fig. 5g, h). Moreover, the number of Fos⁺ neurons within the PBN_{EL}, including a Fos
259 and CGRP double-positive population, correlated with stimulation intensity (Fig. 5h-j),
260 suggesting that neurons within the PBN_{EL} may control behaviors associated with different
261 valences in a scalable manner. Together, these findings indicate that the *Gpr83*⁺ mechanosensory
262 limb of the SPB tract is associated with either positive or negative emotional valence, depending
263 on stimulus intensity.

264

265 **Discussion**

266 While studies of the anterolateral pathway have mainly focused on its role in pain and
267 temperature sensation, subdivisions of the anterolateral pathway that may mediate affective

268 touch have been poorly understood. We propose that the *Gpr83*⁺ SPB pathway is a unique
269 subdivision of the anterolateral pathway that conveys tactile information to higher brain centers
270 via the PBN_L to underlie affective touch (Extended Data Fig. 10a). Support for this model
271 includes the observations that *Gpr83*⁺ SPB neurons are highly sensitive to mechanical stimuli,
272 they receive strong synaptic inputs from primary mechanosensory neurons, and they convey
273 tactile information bilaterally to the PBN_L in a manner that is non-topographically organized. In
274 addition, low-intensity stimulation of *Gpr83*⁺ SPB neurons is appetitive, whereas high-intensity
275 stimulation of these neurons is aversive. It is noteworthy that *Gpr83*⁺ SPB neurons receive
276 synaptic inputs from both LTMRs and HTMRs, suggesting that the *Gpr83*⁺ SPB pathway
277 underlies either positive or negative valence associated with cutaneous mechanosensation
278 depending on the properties or intensity of a tactile stimulus.

279

280 The current view of ascending pain pathways emphasizes the involvement of *Tacr1*⁺ PNs
281 in transmitting nociceptive signals from the spinal cord to the brain. However, therapeutic
282 strategies that target *Tacr1*-expressing neurons and the TACR1 receptor itself to treat pain have
283 been minimally successful²⁸, consistent with the existence of additional, *Tacr1*-negative SPB
284 neurons²⁹. Our physiological and behavioral findings suggest that *Tacr1*⁺ and *Gpr83*⁺ SPB
285 neurons form parallel ascending circuit motifs that cooperate to convey nociceptive signals to the
286 brain (Extended Data Fig. 10a). These two SPB modules receive synaptic inputs from distinct
287 but overlapping sets of nociceptors and project to distinct but overlapping PBN_L subnuclei,
288 which presumably engage different downstream brain regions associated with processing
289 nociceptive signals. Indeed, strong activation of *Tacr1*⁺ and *Gpr83*⁺ SPB neurons generates
290 spatiotemporally distinct patterns of escape locomotion, autonomic (pupillary) reactions, and
291 place aversion, supporting the idea that these two SPB circuit motifs mediate different aspects of
292 pain perception and behavioral responses to noxious stimuli. Intriguingly, TACR1 and GPR83
293 are structurally highly related GPCR family members (Extended Data Fig. 10b), both coupled to
294 G_q signaling pathways³⁰, suggesting that they may modulate the activities of *Tacr1*⁺ and *Gpr83*⁺
295 SPB neurons, respectively. Future studies of the TACR1 and GPR83 GPCRs, and the spinal PNs
296 that express them, may reveal new therapeutic approaches for treating disorders associated with
297 pain and affective touch.

298

299 **References**

- 300 1 Abraira, V. E. & Ginty, D. D. The sensory neurons of touch. *Neuron* **79**, 618-639,
301 doi:10.1016/j.neuron.2013.07.051 (2013).
- 302 2 Basbaum, A. I., Bautista, D. M., Scherrer, G. & Julius, D. Cellular and molecular
303 mechanisms of pain. *Cell* **139**, 267-284, doi:10.1016/j.cell.2009.09.028 (2009).
- 304 3 Todd, A. J. Neuronal circuitry for pain processing in the dorsal horn. *Nature reviews.*
305 *Neuroscience* **11**, 823-836, doi:10.1038/nrn2947 (2010).
- 306 4 Werberger, R. & Basbaum, A. I. Spinal cord projection neurons: a superficial, and also
307 deep analysis. *Current Opinion in Physiology* **11**, 109-115 (2019).
- 308 5 Owens, D. M. & Lumpkin, E. A. Diversification and specialization of touch receptors in
309 skin. *Cold Spring Harb Perspect Med* **4**, doi:10.1101/cshperspect.a013656 (2014).
- 310 6 Haring, M. *et al.* Neuronal atlas of the dorsal horn defines its architecture and links
311 sensory input to transcriptional cell types. *Nat Neurosci* **21**, 869-880,
312 doi:10.1038/s41593-018-0141-1 (2018).
- 313 7 Gong, S. *et al.* A gene expression atlas of the central nervous system based on bacterial
314 artificial chromosomes. *Nature* **425**, 917-925, doi:10.1038/nature02033 (2003).
- 315 8 Huang, T. *et al.* Identifying the pathways required for coping behaviours associated with
316 sustained pain. *Nature* **565**, 86-90, doi:10.1038/s41586-018-0793-8 (2019).
- 317 9 Sabatier, C. *et al.* The divergent Robo family protein rig-1/Robo3 is a negative regulator
318 of slit responsiveness required for midline crossing by commissural axons. *Cell* **117**, 157-
319 169, doi:10.1016/s0092-8674(04)00303-4 (2004).
- 320 10 Bourane, S. *et al.* Gate control of mechanical itch by a subpopulation of spinal cord
321 interneurons. *Science* **350**, 550-554, doi:10.1126/science.aac8653 (2015).
- 322 11 Abraira, V. E. *et al.* The Cellular and Synaptic Architecture of the Mechanosensory
323 Dorsal Horn. *Cell* **168**, 295-310 e219, doi:10.1016/j.cell.2016.12.010 (2017).
- 324 12 Palmiter, R. D. The Parabrachial Nucleus: CGRP Neurons Function as a General Alarm.
325 *Trends Neurosci* **41**, 280-293, doi:10.1016/j.tins.2018.03.007 (2018).
- 326 13 Fulwiler, C. E. & Saper, C. B. Subnuclear organization of the efferent connections of the
327 parabrachial nucleus in the rat. *Brain Res* **319**, 229-259, doi:10.1016/0165-
328 0173(84)90012-2 (1984).
- 329 14 Han, S., Soleiman, M. T., Soden, M. E., Zweifel, L. S. & Palmiter, R. D. Elucidating an
330 Affective Pain Circuit that Creates a Threat Memory. *Cell* **162**, 363-374,
331 doi:10.1016/j.cell.2015.05.057 (2015).
- 332 15 Chiang, M. C. *et al.* Divergent Neural Pathways Emanating from the Lateral Parabrachial
333 Nucleus Mediate Distinct Components of the Pain Response. *Neuron*,
334 doi:10.1016/j.neuron.2020.03.014 (2020).
- 335 16 Langford, D. J. *et al.* Coding of facial expressions of pain in the laboratory mouse. *Nat*
336 *Methods* **7**, 447-449, doi:10.1038/nmeth.1455 (2010).
- 337 17 Craig, A. D., Krout, K. & Andrew, D. Quantitative response characteristics of
338 thermoreceptive and nociceptive lamina I spinothalamic neurons in the cat. *J*
339 *Neurophysiol* **86**, 1459-1480, doi:10.1152/jn.2001.86.3.1459 (2001).
- 340 18 Hachisuka, J. *et al.* Semi-intact ex vivo approach to investigate spinal somatosensory
341 circuits. *Elife* **5**, doi:10.7554/eLife.22866 (2016).
- 342 19 Bester, H., Chapman, V., Besson, J. M. & Bernard, J. F. Physiological properties of the
343 lamina I spinoparabrachial neurons in the rat. *J Neurophysiol* **83**, 2239-2259,
344 doi:10.1152/jn.2000.83.4.2239 (2000).

345 20 Andrew, D. Quantitative characterization of low-threshold mechanoreceptor inputs to
346 lamina I spinoparabrachial neurons in the rat. *J Physiol* **588**, 117-124,
347 doi:10.1113/jphysiol.2009.181511 (2010).

348 21 Liu, Q. *et al.* Molecular genetic visualization of a rare subset of unmyelinated sensory
349 neurons that may detect gentle touch. *Nat Neurosci* **10**, 946-948, doi:10.1038/nn1937
350 (2007).

351 22 Li, L. *et al.* The functional organization of cutaneous low-threshold mechanosensory
352 neurons. *Cell* **147**, 1615-1627, doi:10.1016/j.cell.2011.11.027 (2011).

353 23 Rau, K. K. *et al.* Mrgprd enhances excitability in specific populations of cutaneous
354 murine polymodal nociceptors. *J Neurosci* **29**, 8612-8619,
355 doi:10.1523/JNEUROSCI.1057-09.2009 (2009).

356 24 Kalueff, A. V., Aldridge, J. W., LaPorte, J. L., Murphy, D. L. & Tuohimaa, P. Analyzing
357 grooming microstructure in neurobehavioral experiments. *Nat Protoc* **2**, 2538-2544,
358 doi:10.1038/nprot.2007.367 (2007).

359 25 McGlone, F., Wessberg, J. & Olausson, H. Discriminative and affective touch: sensing
360 and feeling. *Neuron* **82**, 737-755, doi:10.1016/j.neuron.2014.05.001 (2014).

361 26 Foerster, O., Breslau, O., and Gagel, O. Die Vorderseitenstrangdurchschneidung
362 beim Menschen: Eine klinisch-patho-physiologisch-anatomische
363 Studie. *Z. Gesamte Neurol. Psychiatr.* **138**, 1-92 (1932).

364 27 Lahuerta, J., Bowsher, D., Campbell, J. & Lipton, S. Clinical and instrumental evaluation
365 of sensory function before and after percutaneous anterolateral cordotomy at cervical
366 level in man. *Pain* **42**, 23-30, doi:10.1016/0304-3959(90)91087-y (1990).

367 28 Hill, R. NK1 (substance P) receptor antagonists--why are they not analgesic in humans?
368 *Trends Pharmacol Sci* **21**, 244-246 (2000).

369 29 Baseer, N., Al-Baloushi, A. S., Watanabe, M., Shehab, S. A. & Todd, A. J. Selective
370 innervation of NK1 receptor-lacking lamina I spinoparabrachial neurons by presumed
371 nonpeptidergic Adelta nociceptors in the rat. *Pain* **155**, 2291-2300,
372 doi:10.1016/j.pain.2014.08.023 (2014).

373 30 Gomes, I. *et al.* Identification of GPR83 as the receptor for the neuroendocrine peptide
374 PEN. *Science signaling* **9**, ra43, doi:10.1126/scisignal.aad0694 (2016).

375 **Figure Legends**

376

377 **Figure 1. *Tacr1*- and *Gpr83*-expressing spinal PNs are largely distinct neuronal populations**

378 **that innervate multiple distinct but overlapping brain regions. a**, Distribution of *Tacr1*⁺

379 neurons in the spinal cord dorsal horn. I_o, outer lamina II; I_{id}, inner dorsal lamina II; LSN,

380 lateral spinal nucleus. **b**, Distribution of GFP-expressing *Gpr83*⁺ neurons in the spinal cord

381 dorsal horn (left). A subset of SPB neurons labeled with CTB555 injected into the PBN_L are

382 GFP-positive (right). Arrow heads, double-positive neurons. **c-d**, Axonal projections of *Tacr1*⁺

383 or *Gpr83*⁺ spinal PNs. PVT, paraventricular nucleus; CM, central medial nucleus; MD,

384 mediodorsal nucleus; PO, posterior complex; VPM, ventral posteromedial nucleus;

385 MG(d)(v)(m), medial geniculate complex (dorsal)(ventral)(medial); SPFp, parvocellular

386 subparafascicular nucleus; SCP, superior cerebellar peduncle. **e**, Quantification of the average

387 fluorescence intensity of tdTomato-expressing *Tacr1*⁺ and *Gpr83*⁺ spinal PN axons in the major

388 brain targets. n = 3 mice. Error bars, s.e.m. **f**, Schematic of virus injections for retrograde

389 labeling of *Tacr1*⁺ spinal PNs. **g**, Distribution of tdTomato-expressing *Tacr1*⁺ spinal PNs and

390 GFP-expressing *Gpr83*⁺ neurons in the spinal cord dorsal horn. Arrowheads, double-positive

391 neurons. **h**, Quantification of co-expression of tdTomato and GFP. n = number of mice

392 (indicated in the bar graphs).

393

394 **Figure 2. Axons of *Tacr1*- and *Gpr83*-expressing SPB neurons terminate in a zonally-**

395 **segregated manner within the PBN_L and their strong activation produces distinct escape**

396 **behaviors and autonomic responses. a**, Distribution of synaptic terminals originating from the

397 spinal cord. n = 2 mice. **b**, Schematic of virus injections. **c**, Distribution of synaptic terminals of

398 *Tacr1*⁺ and *Gpr83*⁺ SPB neurons in the PBN_L. **d**, Quantification. n = 5, 4 mice for *Tacr1*⁺,

399 *Gpr83*⁺ SPB neurons, respectively. **e**, Top, schematic of optogenetic stimulation of SPB axonal

400 terminals. Bottom, representative PBN_L images for fiberoptic implant sites. n = 5, 8 mice for

401 *Tacr1*⁺, *Gpr83*⁺, respectively. **f**, Distribution of Fos⁺ neurons in the PBN_L following high-power

402 (6.5 mW) photostimulation. **g**, Quantification of the number of Fos⁺ neurons in different PBN_L

403 subnuclei. One-way ANOVA (Dunnett's multiple comparisons test); $F_{[2, 8]} = 11.70$ (PBN_{CL}), $F_{[2,$

404 $8]} = 8.58$ (PBN_{IL}), $F_{[2, 8]} = 21.21$ (PBN_{DL}), $F_{[2, 8]} = 63.00$ (PBN_{EL}); n = 4, 4, 3 mice for control,

405 *Tacr1*, and *Gpr83*, respectively. **h**, Speed of movement over time. Turquoise bars, 30-second-

406 long light-on periods (473 nm, 6.5 mW, 5 Hz, 10 ms pulse width). Shaded areas, s.e.m. **i, j**,
407 Quantifications of average speed (i) and number of jumps (j) during light-on (6.5 mW) periods.
408 One-way ANOVA (Dunnett's multiple comparisons test); $F_{[2, 16]} = 21.32$ (5 Hz), $F_{[2, 16]} = 31.05$
409 (10 Hz) (i); $F_{[2, 16]} = 6.53$ (10 Hz) (j); n = 8, 6, 5 mice for control, *Tacr1*, and *Gpr83*, respectively.
410 **k, l**, Quantification of average speed (n) or number of jumps (o) during light-on (10 Hz) periods
411 following NBQX (or saline) pre-infusion into the PBNL. Paired *t*-test (two-tailed). **m**, Relative
412 change in pupil diameter over time ($\Delta D/D$, see methods for calculation). Inset, representative
413 pupil images during baseline (top) and light-on (bottom) periods. Turquoise bars, 10-second-long
414 light-on periods (473 nm, 2 mW, 10 Hz, 10 ms pulse width). Shaded areas, s.d. Note that abrupt
415 downward lines in the shaded regions reflects blinking/squinting. **n-p**, Quantifications of peak
416 amplitude (n), area under curve (o), and number of blinks/squints (p). One-way ANOVA
417 (Tukey's multiple comparisons test); $F_{[2, 15]} = 30.44$ (peak amplitude), $F_{[2, 15]} = 21.11$ (area under
418 curve), $F_{[2, 17]} = 7.412$ (blinks/squints); n = 6, 7, 5 mice for control, *Tacr1*, *Gpr83*, respectively.
419 Error bars, s.e.m.

420

421 **Figure 3. *Tacr1*- and *Gpr83*-expressing SPB neurons exhibit different responses to**
422 **cutaneous stimuli, which is explained by their distinct synaptic inputs from primary**
423 **sensory neuron subtypes. **a****, Schematic of whole-cell patch clamp recordings from *Tacr1*⁺ and
424 *Gpr83*⁺ SPB neurons using an *ex vivo* skin-spinal cord preparation. **b, c**, Representative traces of
425 action potential (AP) firing evoked by von Frey filament indentations (b) and saline application
426 with different temperatures (c). Underbars, time when stimuli were applied to the skin. **d**,
427 Summary radar plots. **e-g**, Quantifications of peak instantaneous firing rates following
428 application of mechanical (e) and temperature (innocuous (f) and noxious (g)) stimuli. Mann-
429 Whitney test (two-tailed) (comparison for individual stimuli); Two-way ANOVA (comparison
430 for different groups of stimuli), $F_{[1, 29]} = 9.77$ (e), $F_{[1, 57]} = 4.41$ (f); n = 16, 15 neurons for *Tacr1*⁺,
431 *Gpr83*⁺, respectively. **h**, Schematic of whole-cell patch clamp recordings from *Tacr1*⁺ and
432 *Gpr83*⁺ SPB neurons using a spinal cord slice preparation. The genetic labeling strategies are
433 described in the methods. **i**, Representative images of tdTomato-expressing *Tacr1*⁺ and *Gpr83*⁺
434 SPB neurons in acute spinal cord slices. n = 39, 35 neurons for *Tacr1*⁺, *Gpr83*⁺, respectively. **j, l**,
435 **n**, Representative traces of light-activated currents (left) and AP firing (right) upon
436 photostimulation of CGRP⁺ (j), *Mrgprb4*⁺ (l), and *Ntrk2*⁺ (n) primary afferent terminals. The

437 light-activated EPSCs were abolished in the presence of tetrodotoxin (TTX) and reinstated in the
438 presence of 4-aminopyridine (4-AP) in addition to TTX, indicating the monosynaptic nature of
439 the synaptic connections. Turquoise bars, 0.1 ms (EPSCs) and 1 ms (APs) LED (473 nm)
440 stimulations. **k, m, o**, Quantifications of peak current density. Mann-Whitney test (two-tailed); n
441 = number of neurons. Error bars, s.e.m.

442

443 **Figure 4. *Tacr1*- and *Gpr83*-expressing SPB neurons form dedicated, bilateral, non-**
444 **somatotopically organized synaptic inputs to the PBN_L.** **a, c**, Schematics of unilateral lumbar
445 injections of AAV viruses for whole-mount AP staining. **b**, Top view of whole-mount AP-
446 stained axonal projections of densely labeled *Tacr1*⁺ and *Gpr83*⁺ spinal PNs. **d**, Single axon
447 traces of sparsely labeled *Tacr1*⁺ and *Gpr83*⁺ SPB neurons. r, rostral; c, caudal, d, dorsal; v,
448 ventral. **e, f**, Quantifications of the numbers of SPB neurons that exhibit dedicated vs. collateral-
449 forming axons (e) and SPB neurons that innervate the PBN_L contralaterally, ipsilaterally, or
450 bilaterally (f). **g**, Schematic of virus injections. **h, i**, Synaptic terminals of *Tacr1*⁺ (h) or *Gpr83*⁺
451 (i) SPB neurons representing hindlimb regions (GFP), thoracic body regions (BFP), and forelimb
452 regions (tdTomato), are intermingled within their respective PBN_L target subnuclei. n = 3 mice
453 each for *Tacr1*⁺ and *Gpr83*⁺ SPB neurons.

454

455 **Figure 5. Activation of *Tacr1*- and *Gpr83*-expressing SPB neurons induces distinct affective**
456 **behaviors in a stimulus intensity-dependent manner.** **a**, Schematic of the optogenetic
457 stimulation-coupled real-time place preference assay. **b, c**, Quantifications of % of time spent in
458 stimulated side for 6.5 mW (b) and 1 mW (c) photostimulations (10 Hz, 10 ms pulse width).
459 One-way repeated measures ANOVA (Dunnett's multiple comparisons test); $F_{[1.626, 8.131]} = 19.10$
460 (*Tacr1*), $F_{[1.580, 7.901]} = 14.41$ (*Gpr83*) (b); $F_{[1.903, 13.32]} = 7.20$ (*Tacr1*), $F_{[1.817, 12.72]} = 8.42$ (*Gpr83*)
461 (c); n = number of mice. **d**, Schematic of the optogenetic stimulation-coupled lever-pressing
462 assay. Mice received 5 second-long photostimulation (473 nm, 10 Hz, 10 ms pulse width) upon
463 pressing an active lever. **e, f**, Fold changes of number of lever press are plotted over sessions.
464 Turquoise boxes, 8 days of light-on sessions. n = 7 (control, 0.4 mW; *Tacr1*, 0.4 mW; *Gpr83*, 0.4
465 mW; *Tacr1*, 1 mW), n = 6 (control, 1 mW), n = 8 mice (*Gpr83*, 1 mW). Two-way repeated
466 measures ANOVA; $F_{[1, 12]} = 5.26$ (0.4 mW), $F_{[1, 12]} = 5.22$ (1 mW) (e); $F_{[1, 12]} = 2.50$ (0.4 mW),
467 $F_{[1, 11]} = 10.14$ (1 mW). **g**, Distribution of Fos⁺ neurons in the PBN_{EL} following photostimulation

468 of *Gpr83*⁺ SPB axon terminals. **h-j**, Quantifications of the number of Fos⁺ neurons in different
469 PBN_L subnuclei (h), % of CGRP⁺ neurons that are Fos⁺ (i), and % of Fos⁺ neurons that are
470 CGRP⁺ (j). One-way ANOVA (Tukey's multiple comparisons test); $F_{[2, 8]} = 7.41$ (PBN_{IL}), $F_{[2, 8]}$
471 $= 22.03$ (PBN_{DL}), $F_{[2, 8]} = 64.36$ (PBN_{EL}); $F_{[2, 8]} = 74.94$ (i); $n = 4, 4, 3$ mice for control, 0.4 mW,
472 and 6.5 mW, respectively. Error bars, s.e.m.

473 **Methods**

474

475 **Mice.** Mice were handled and housed in accordance with Harvard Medical School and IACUC
476 guidelines. Mice were kept in a temperature- and humidity-controlled room with a 12-hour
477 light/dark cycle. Mice (2-24 weeks of age) from both genders were used in experiments. Knockin
478 mouse lines generated in this study include the *Robo3*^{IRES-CreERT2}, *Tacr1*^{CreERT2}, *Gpr83*^{CreERT2},
479 *Advillin*^{FlpO}, and *Tau*^{FSFIAP} (this mouse line will be described elsewhere) mouse lines. These
480 knockin mouse lines were generated in the Janelia Research Campus Gene Targeting and
481 Transgenic Facility using conventional ES cell targeting strategies. Briefly, a 3X-STOP-IRES-
482 CreERT2 cassette was introduced via homologous recombination into the first common coding
483 exon that is shared by different splice variants of the *Robo3* gene for the *Robo3*^{IRES-CreERT2}
484 knockin mouse line. CreERT2 cassettes were introduced via homologous recombination into the
485 *Tacr1*, *Gpr83*, and *Advillin* genes, replacing the first coding ATGs to generate the *Tacr1*^{CreERT2},
486 *Gpr83*^{CreERT2}, and *Advillin*^{FlpO} mouse lines, respectively. Detailed sequence elements of the
487 targeting vectors are described in Extended Data Fig. 1a. *Robo3*^{IRES-CreERT2}, *Tacr1*^{CreERT2},
488 *Gpr83*^{CreERT2}, and *Advillin*^{FlpO} heterozygous mice were generated by mating chimeric mice to
489 germline FlpE (*Actb-FlpE*) (JAX#003800) or germline Cre (*EIIa-Cre*) (JAX#003724) mice to
490 remove the neomycin selection cassette. Other published knockin mouse lines used in this study
491 include *Lbx1*^{FlpO} 10, *Rosa26*^{FSF-LSL-tdTomato} (Ai65) (JAX#021875), *Rosa26*^{LSL-tdTomato} (Ai14)
492 (JAX#007908), *Rosa26*^{LSL-EYFP} (Ai3) (JAX#007903), *Rosa26*^{LSL-synaptophysin-tdTomato} (Ai34)
493 (JAX#012570), *Rosa26*^{FSF-tdTomato} (generated from the cross between Ai65 and *EIIa-Cre* mouse
494 lines; germline excision of LSL), *Rosa26*^{LSL-FSF-ReaChr 31} (JAX#024846), *Rosa26*^{LSL-FSF-TeTx 32},
495 *Rosa26*^{FSF-LSL-Synaptophysin-GFP 33}, *Tacr1*^{IRES2-Cre} (JAX#021877), *Gad2*^{NLS-mCherry} (JAX#023140),
496 *Advillin*^{Cre 34}, *Ntrk2*^{CreER 35}, *Mrgprb4*^{Cre 36}, and *Mrgprd*^{Cre 23}. The *Calca-FlpE* BAC transgenic
497 mouse line was generated by introducing a FlpE cassette downstream of the first coding ATG of
498 the *Calca* gene in a bacterial artificial chromosome (RP23-181A2). The *Gpr83-EGFP* BAC
499 transgenic mouse line was imported from the MMRRC (Stock number: 010442-UCD). Other
500 published transgenic mouse lines used in this study include *Cdx2-Cre* (JAX#009352), *Calca-*
501 *GFP* (MMRRC, Stock number: 011187-UCD) and *Cdx2-NSE-FlpO*¹¹.

502

503 **Tamoxifen treatment.** Tamoxifen (T5648, Sigma) was dissolved in 100% ethanol (20 mg/ml),
504 mixed with a 2x volume of sunflower seed oil (S5007, Sigma), vortexed for 20 minutes and
505 vacuum centrifuged for 30 minutes for ethanol evaporation. Tamoxifen in sunflower seed oil (10
506 mg/ml) was delivered via oral gavage to pregnant female mice for embryonic treatment (3-4 mg
507 at E11.5 for *Robo3^{CreERT2}*) or to mice at weaning ages (P19-P24) for postnatal treatments (1-1.5
508 mg for *Tacr1^{CreERT2}* and 2-2.5 mg *Gpr83^{CreERT2}*). The number of tamoxifen treatments for
509 *Tacr1^{CreERT2}* and *Gpr83^{CreERT2}* varied depending on reporter mouse lines and Cre-dependent
510 viruses used for experiments; *Rosa26^{FSF-LSL-tdTomato}* (Ai65), *Rosa26^{LSL-tdTomato}* (Ai14), and
511 *Rosa26^{LSL-EYFP}* (Ai3), *Tau^{FSFIAP}*, one dose; *Rosa26^{LSL-FSF-ReaChr}*, two doses two days apart;
512 *Rosa26^{LSL-FSF-TeTx}*, three doses on three consecutive days; AAV1-FLEX-PLAP, one dose 5-7
513 days after virus injection; all other Cre-dependent viruses, two to three doses were administered
514 5-14 days after virus injections.

515

516 **Surgical procedures. Spinal cord injections.** Mice (P12-20) were anesthetized via continuous
517 inhalation of isoflurane (1.5 – 2.5 %) using an isoflurane vaporizer (VetEquip) during the
518 surgery. Laminectomies were performed to expose either cervical, thoracic, or lumbar spinal
519 cords, and total 300 – 450 nl of AAV viruses were directly injected into two to three adjacent
520 spots in the spinal cord using pulled glass pipettes (Wiretrol II, Drummond) and a microsyringe
521 pump injector (UMP3, World Precision Instruments). For sparse labeling experiments described
522 in Fig. 4, 150 nl of 1/10 diluted AAV1-hSyn-FlpO-WPRE (1.37E+12gc/ml) was injected into
523 one location in the lumbar spinal cord.

524 **Brain injections and fiberoptic/dual opto-fluid cannula implants.** Mice (6-10 weeks old) were
525 placed on a stereotaxic frame (Kopf Instruments) and anesthetized via continuous inhalation of
526 isoflurane (1.5 – 2.5 %) using an isoflurane vaporizer during the surgery. Burr holes were made
527 on the skull using a dental drill, and 150 – 250 nl of Alexa Fluor-conjugated CTB
528 (ThermoFisher) or 100 – 300 nl of AAV viruses were injected into the target brain regions using
529 pulled glass pipettes (Wiretrol II, Drummond) and a microsyringe pump injector (UMP3, World
530 Precision Instruments). For fiberoptic or dual opto-fluid cannula implants, fiberoptic cannulas
531 (400 µm in diameter, 0.53NA, Doric Lenses) or dual opto-fluid cannulas (DiOFC, Doric Lenses)
532 were bilaterally implanted into the PBNL and secured using a gel type super glue (Loctite) with
533 an accelerator application followed by dental cement (Metabond, Parkell) application. The

534 coordinates used for stereotaxic injections/implants are as follows; PBN_L (-5.2 – -5.0 mm
535 posterior to bregma, ± 1.4 – 1.6 mm from midline, and -2.8 – -3.0 ventral to dura), MGm/SPFp
536 (-3.05 – -3.15 mm posterior to bregma, -1.70 – -1.75 mm from midline, and -3.0 – -3.2 mm
537 ventral to dura), SCig (-3.35 – -3.50 mm posterior to bregma, -0.75 – -1.25 mm from midline,
538 and -1.35 – -1.45 mm ventral to dura).

539

540 **Viruses.** The following AAV viruses were used in this study: AAV1-CAG-FLEX-
541 Synaptophysin-GFP-WPRE (1.088E+14gc/ml), AAV1-CAG-FLEX-Synaptophysin-BFP-WPRE
542 (1.5059E+14gc/ml), AAV1-CAG-FLEX-Synaptophysin-tdTomato-WPRE (1.1482E+14gc/ml),
543 AAV2-Retro-CAG-FLEX-tdTomato-WPRE (2.22248E+13gc/ml), AAV2-Retro-EF1 α -FlpO-
544 WPRE (2.683E+13gc/ml), AAV1-hSyn-Con/Fon-EYFP-WPRE (1.04E+13gc/ml), and AAV1-
545 hSyn-FlpO-WPRE (1.37E+13gc/ml). pAAV-FLEX-Synaptophysin-GFP expression vector³⁷ was
546 a gift from Silvia Arber. pAAV-FLEX-Synaptophysin-BFP and pAAV-FLEX-Synaptophysin-
547 tdTomato expression vectors were generated by swapping the GFP sequence with BFP and
548 tdTomato sequences, respectively. pAAV-CAG-FLEX-Synaptophysin-tdTomato-WPRE
549 (Addgene#51503) and pAAV-hSyn-Con/Fon-EYFP-WPRE³⁸ (Addgene#55650) expression
550 vectors were purchased from Addgene. pAAV-EF1 α -FlpO-WPRE and pAAV-hSyn-FlpO-
551 WPRE expression vectors were generated using standard approaches. All the AAV viruses were
552 produced and packaged at the Boston Children's Hospital Viral Core Facility except for the
553 AAV1-FLEX-PLAP virus, which was a gift from Connie Cepko.

554 *Dual-virus retrograde labeling experiments.* The traditional view of the anterolateral pathway is
555 that most of the spinal PN axons form collateral branches that innervate multiple regions of the
556 brain, including the PBN_{L3}; this is based on double labeling of neurons by retrograde tracers
557 injected into different brain regions. However, one potential caveat of this approach is that some
558 brain targets of the anterolateral pathway, particularly in the hindbrain, including the PBN_L of
559 the pons and brainstem, are located near main bundles of ascending anterolateral pathway axons,
560 potentially complicating interpretation of retrograde labelling experiments because PNs may be
561 labelled by uptake of tracers into fibers of passage as well as axon terminals. To circumvent this
562 concern, we selectively labeled *Tacr1*⁺ or *Gpr83*⁺ spinal PNs that innervate rostral brain targets,
563 including the MGm/SPFp of the posterior thalamus and the SCig of the midbrain, by combining

564 lumbar spinal cord injections of AAV1-Con/Fon-EYFP viruses³⁸ and brain injections of AAV2-
565 retro-FlpO viruses³⁹ into *Tacr1CreERT2* or *Gpr83CreERT2* mice (Extended Data Fig. 3).
566 *AAV1-FLEX-Synaptophysin virus injections into three spinal axial levels.* AAV1-FLEX-
567 Synaptophysin viruses³⁷ expressing one of three different fluorescent proteins (GFP, BFP, and
568 tdTomato) were injected into three spinal axial levels (lumbar enlargement, mid-thoracic, and
569 cervical enlargement) of either *Tacr1CreERT2* or *GPR83CreERT2* mice to visualize synaptic terminals
570 of SPB neurons representing hindlimbs, thoracic body regions, and forelimbs, respectively
571 (Figure 4g-i, Extended Data Figure 8f).

572

573 **RNAscope *in situ* hybridization.** Adult mice were euthanized with carbon dioxide. Lumbar
574 spinal cords were dissected and immediately embedded in OCT (1437365, Fisher) and frozen
575 with dry ice-cooled methylbutane. The spinal cord tissues were cyrosectioned (25 μ m) using a
576 cryostat (Leica), and transverse sections were collected on glass slides (12-550-15, Fisher).
577 mRNA transcripts were detected using RNAscope Fluorescent Multiplex Assay (Advanced Cell
578 Diagnostics) and RNAscope Fluorescent Multiplex Reagent Kit (Cat. No. 320850). The
579 RNAscope catalog probes were used to detect *Gpr83* (Cat. No. 317431), *Tac1* (Cat. No. 410351)
580 and *tdTomato* (Cat. No. 317041-C2) mRNA molecules.

581

582 **Immunohistochemistry.** Mice (6 – 8 weeks old) were anesthetized with CO₂ and transcardially
583 perfused with 5-10 mL of modified Ames Media (A1420, Sigma) in 1x PBS, followed by 20-30
584 mL of 4% paraformaldehyde (PFA) (P6148, sigma or 15714-S, EMS) in 1x PBS at room
585 temperature (RT). Brains and vertebral columns, including spinal cords and dorsal root ganglia,
586 were roughly dissected from perfused mice and post-fixed in 4% PFA at 4°C overnight. Tissues
587 were washed in 1x PBS for over 3 hours, and brains and spinal cords were finely dissected out
588 from the rest of the tissue. Brain and spinal cord tissues were cryoprotected in 30% sucrose in 1x
589 PBS at 4°C for 2 days, embedded in OCT (1437365, Fisher), frozen using dry ice, and kept at -
590 80°C. Brain (coronal sections) and spinal cord (transverse or horizontal sections) tissues were
591 cyrosectioned (30 - 40 μ m) using a cryostat (Leica). Spinal cord sections were collected on glass
592 slides (12-550-15, Fisher) and brain sections were collected on glass slides or in 1x PBS.
593 Sections (on slides for spinal cord sections, on slides or as floating sections for brain sections)
594 were washed 3 times for 5 minutes each with 1x PBS containing 0.1% Triton X-100 (0.1%

595 PBST), incubated with blocking solutions (0.1% PBST containing 5% normal goat serum (S-
596 1000, Vector Labs) or normal donkey serum (005-000-121, Jackson Immuno)) for 1 hour at RT,
597 incubated with primary antibodies diluted in blocking solutions at 4°C overnight, washed 3 times
598 for 10 minutes each with 0.1% PBST, incubated with secondary antibodies diluted in blocking
599 solutions at 4°C overnight, washed again 4 times for 10 minutes each with 0.1% PBST (DAPI
600 solution (D1306, ThermoFisher) was included in the second wash at 1:5000 dilution), and
601 mounted with fluoromount-G (Southern Biotech). IB4 (Alexa 647 conjugated, I32450,
602 ThermoFisher) was diluted at 1:300 and incubated together with secondary antibodies. Primary
603 antibodies used in this study include rabbit anti-DsRed (1:1000, 632496, Clontech), goat anti-
604 mCherry (1:1000, AB0040-200, Acris), chicken anti-GFP (1:1000, GFP-1020, Aves Labs),
605 rabbit anti-GFP (1:1000, A-11122, Life Technologies), mouse anti-NeuN (1:1000, MAB377,
606 Millipore), rabbit anti-tagRFP (for BFP detection, 1:1000, AB233, Evrogen), rabbit anti-TACR1
607 (1:2000, S8305, Sigma), rabbit anti-PKC γ (1:1000, SC-211, Santa Cruz Biotechnology), mouse
608 anti-c-Fos (1:1000, M-1752-100, Biosensis), rabbit anti-phospho-c-Fos (1:500, #5348, Cell
609 Signaling), and rabbit anti-CGRP (1:1000, 24112, Immunostar). Secondary antibodies included
610 Alexa 488 or 546 conjugated goat anti-rabbit antibodies, Alexa 488 or 546 conjugated goat anti-
611 chicken antibodies, Alexa 488 or 647 conjugated goat anti-mouse antibodies (IgG₁), Alexa 647
612 conjugated goat anti-guinea pig antibodies, Alexa 488 conjugated donkey anti-chicken
613 antibodies, Alexa 546 conjugated donkey anti-goat antibodies, and Alexa 488 or 647 conjugated
614 donkey anti-rabbit antibodies. All secondary antibodies were purchased from Life Technologies
615 except for Alexa 488 conjugated donkey anti-chicken antibodies, which was purchased from
616 Jackson ImmunoResearch, and used at 1:500 dilution.

617

618 **Whole-mount alkaline phosphatase (AP) staining.** Mice (6 – 8 weeks old) were euthanized,
619 perfused, fixed, and dissected as described in the immunohistochemistry section. Cortexes and
620 cerebellums were removed, and the remaining tissues, including subcortical regions of the brain
621 and spinal cords, were subjected to heat inactivation of endogenous AP for 2-5 hours at 65-68°C
622 in 1x PBS. The tissues were washed with B1 buffer (0.1 M Tris pH 7.5, 0.15 M NaCl) 3 times
623 for 10 minutes each at RT and then washed with B3 buffer (0.1 M Tris pH 9.5, 0.1 M NaCl, 50
624 mM MgCl₂, 0.1% Tween-20) 3 times for 10 minutes each at RT. The tissues were then incubated
625 with B3 buffer containing NBT(11383213001, Sigma)/BCIP(11383221001, Sigma) (diluted at

626 3.4 µg/ml each) 0.5 – 1.5 days at RT for AP reactions. The next day, tissues were washed with
627 1x PBS, fixed with 4% PFA in 1x PBS for over 4 hours at 4°C, serially dehydrated with 50%,
628 75%, and 100% methanol for 1 hour each, and incubated in fresh 100% methanol overnight.
629 Dehydrated tissues were pinned to a glass dish coated with Sylgard (Sylgard 184 Silicone
630 Elastomer Kit (Dow)), cleared in BABB (BABB: 1 part Benzyl Alcohol (108006, Sigma): 2
631 parts Benzyl Benzoate (B6630, Sigma)) for 10 - 30 minutes, and then imaged.

632

633 **Imaging and image analyses.** *Fluorescence images.* Z-stack images were taken with a Zeiss
634 LSM 700 confocal microscope using either 10X (Plan-Apochromat 10X/NA 0.45) or 20X (Plan-
635 Apochromat 20X/NA 0.8) objectives. The Tile-scan function was used for imaging large spinal
636 cord and brain sections, and the tile images were stitched using Zeiss Zen microscope software.
637 Fluorescence overlaps (Fig. 1g, h, Extended Data Fig. 1b, c, e, f, 2a-f, j-n, 8b, c), the number of
638 cell bodies of SPB neurons (Extended Data Fig. 7h, i), and the number of Fos⁺ neurons (Fig. 2f,
639 g, 5g-j, Extended Data Fig. 4g, h, 6e, f) were analyzed using either Zeiss Zen microscope
640 software (2.3 SP1) or ImageJ (2.0.0-rc-69/1.52p) with Cell Counter plugin mostly by
641 investigators who were blinded to genotype. Average fluorescence intensity of tdTomato⁺ axons
642 (Fig. 1c-e), fluorescence densities of synaptic terminals in the subnuclei of PBN_L (Fig. 2c, d,
643 Extended Data Fig. 2p, q) and dendritic lengths of SPB neurons (Extended Data Fig. 7h, j, k)
644 were measured using ImageJ. The number of tdTomato⁺ synaptic terminals of SPB axons
645 associated with GFP⁺ cell bodies and neurites (Extended Data Fig. 4a, b) was quantified using
646 custom image analysis modules built with CellProfiler software (3.1.9). The estimation of the
647 percentages of spinal cord *Tacr1*⁺ and *Gpr83*⁺ neurons that constitute anterolateral pathway PNs
648 (described in the Extended Data Fig. 6 figure legend) were calculated based on retrograde
649 labeling experiments described in Extended Data Fig. 2e. However, the estimated percentages
650 are lower bounds and almost certainly underestimations because it is unlikely that 100% labeling
651 efficiency was achieved with retrograde tracer injections and because injecting retrograde tracers
652 into all the brain targets of the anterolateral pathway was not feasible.

653 *Bright field images of whole-mount AP stained tissues.* Bright field images of whole-mount AP
654 stained tissues were taken with a Zeiss Axio Zoom.V16 microscope using a 1X objective
655 (PlanNeoFluar Z 1.0x/0.25 FWD 56mm). Sparsely labeled single axons of SPB neurons (Fig. 4d-
656 f) were traced using ImageJ with Simple Neurite Tracer plugin.

657

658 **Fos induction measurements.** Mice were acclimated in stimulation chambers for two days (20 –
659 30 minutes each day) before the test day. For high-intensity optogenetic stimulation of SPB axon
660 terminals (Fig. 2f, g, Fig. 5g-j, Extended Data Fig. 4g, h), 6.5 mW blue light (473 nm, 10 Hz, 10
661 ms pulse width) was delivered through fiberoptic cannulas implanted in the PBN_L four times for
662 30 seconds each (30 second light-off periods between photostimulation periods). For low-
663 intensity photostimulation (Fig. 5g-j), 0.4 mW blue light (473 nm, 10 Hz, 10 ms pulse width)
664 was delivered either four times for 30 seconds each (30 second light-off periods between
665 photostimulation periods) or 16 times for five seconds each (10 second light-off periods between
666 photostimulation periods). Littermate controls were photostimulated with either of the protocols
667 above. For thermal stimulation (Extended Data Fig. 6e, f), mice were placed either on a 55°C hot
668 plate for 30 seconds or on a 5°C cold plate for 10 minutes. Littermate controls were placed on a
669 plate at room temperature for 10 minutes. 1.5 hours after the delivery of each stimulation, mice
670 were perfused and processed for Fos immunohistochemical analysis.

671

672 ***Ex vivo* whole-cell patch-clamp recordings using a skin-spinal cord preparation.** A semi-
673 intact skin-spinal cord preparation was used as previously described¹⁸ with a few modifications.
674 Briefly, mice (6–9 weeks old) were deeply anesthetized with ketamine/xylazine (90 and 10
675 mg/kg, respectively) and transcardially perfused through the left ventricle with oxygenated (95%
676 O₂ and 5% CO₂) sucrose-based artificial cerebrospinal fluid (ACSF) (in mM; 234 sucrose, 2.5
677 KCl, 0.5 CaCl₂, 10 MgSO₄, 1.25 NaH₂PO₄, 26 NaHCO₃, 11 Glucose) at room temperature.
678 Immediately after perfusion, the skin was incised along the dorsal midline and the spinal cord
679 was quickly exposed via dorsal laminectomy. The right hindlimb and the spinal cord (~C2 – S6)
680 were dissected, transferred onto Sylgard-coated dissection/recording dish, and submerged in the
681 same sucrose-based ACSF, which was circulated at 50 ml/min for superfusion of the spinal cord.
682 Next, the skin piece innervated by the saphenous nerve and the femoral cutaneous nerve was
683 dissected free of surrounding tissues. The L2 and L3 DRGs were left attached on the spine. Dural
684 and pial membranes were carefully removed and the spinal cord was pinned onto the Sylgard
685 chamber with the right dorsal horn facing upward. After the dissection, the chamber was
686 transferred to the electrophysiology rig, and the skin-spinal cord preparation was perfused with
687 normal ACSF solution (in mM; 117 NaCl, 3.6 KCl, 2.5 CaCl₂, 1.2 MgCl₂, 1.2 NaH₂PO₄, 25

688 NaHCO₃, 11 glucose) saturated with 95% O₂ and 5% CO₂ at 32°C. The tissues were rinsed with
689 ACSF for at least 30 minutes to wash out sucrose. Thereafter, recordings were performed for up
690 to 6 hours post-dissection. Neurons were visualized using a fixed stage upright microscope
691 (BX51WI, Olympus) equipped with a 40X water immersion objective and a CCD camera
692 (ORCA-ER, Hamamatsu Photonics). A narrow beam infrared LED (L850D-06, Marubeni) was
693 positioned outside the solution meniscus. Either *Tacr1*⁺ or *Gpr83*⁺ lamina I SPB neurons were
694 identified by CTB (injected into the PBN_L) and GFP (or tdTomato) double fluorescence. Whole-
695 cell patch-clamp recordings were then performed using a thin-walled single-filamented
696 borosilicate glass pipette pulled with a microelectrode puller (PC-10, Narishige International).
697 The Pipette resistance ranged from 6 to 12 MΩ. Electrodes were filled with an intracellular
698 solution (in mM: 135 K-gluconate, 5 KCl, 0.5 CaCl₂, 5 EGTA, 5 HEPES, 5 MgATP, pH 7.2).
699 Signals were acquired using a Axopatch 200B amplifier (Molecular Devices). The data were
700 low-pass filtered at 2 kHz and digitized at 10 kHz with an A/D converter (Digidata 1322A,
701 Molecular Devices) and stored using a data acquisition program (Clampex version 10, Molecular
702 Devices). The liquid junction potential was not corrected. To search for a cell's receptive field,
703 mechanical stimulation with a firm brush or thermal stimulation with hot (50°C) or cold (0°C)
704 saline was applied systematically over the skin. Once a receptive field was located, stimuli were
705 reapplied directly to the receptive field. To record action potential firings following mechanical
706 stimulation, the skin was indented using a range of von Frey filaments (0.16g, 1g, 2g and 4g). To
707 record action potential firings following application of thermal stimuli, saline with various
708 temperatures (0°C, 15°C, 40°C and 54°C) was gently applied to the skin using a 10 ml syringe.
709 To record capsaicin-evoked action potential firings, 0.05% capsaicin (20 μl) dissolved in 100%
710 ethanol was gently applied to the skin. Peak instantaneous firing frequency was used to evaluate
711 the response to each stimulus. The baseline firing rate (average spontaneous firing rate before
712 stimulus) was subtracted from the peak instantaneous firing frequency. Cells that exhibited peak
713 instantaneous firing frequency greater than 2 Hz were counted as responders.

714

715 **Whole-cell patch-clamp recordings using an acute spinal cord slice preparation.** ReaChR, a
716 red-shifted variant of channelrhodopsin₄₀, was selectively expressed in distinct primary sensory
717 neuron subtypes using intersectional genetic strategies that combine a sensory neuron subtype
718 specific Flp (or Cre) recombinase mouse line, a pan-sensory neuron-specific *Advillin*^{Cre} line³⁴ (or

719 a newly generated *Advillin^{FlpO}* line) (Extended Data Fig. 1e, 7a), and the dual recombinase
720 dependent ReaChR mouse line *Rosa26^{LSL-FSF-ReaChR}* (Fig. 3h). Whole-cell patch-clamp recordings
721 were then performed on *Gpr83⁺* and *Tacr1⁺* SPB neurons labeled with tdTomato by viral
722 delivery of AAV2-Retro-FLEX-tdTomato into the PBN_L of quadruple transgenic mice harboring
723 either the *Tacr1^{CreERT2}* or *Gpr83^{CreERT2}* allele. Acute transverse spinal cord slices were used for
724 whole-cell patch-clamp recordings of retrogradely labeled *Tacr1⁺* and *Gpr83⁺* SPB neurons.
725 Specifically, mice (5-7 weeks old) were anesthetized via continuous inhalation of isoflurane
726 (1.5% – 2.5%) while vertebral columns were dissected. Lumbar enlargements were dissected out
727 from vertebral columns in an ice-cold choline solution (in mM: 92 Choline Chloride, 2.5 KCl,
728 1.2 NaH₂PO₄, 30 NaHCO₃, 20 HEPES, 25 Glucose, 5 Sodium Ascorbate, 2 Thiourea, 3 Sodium
729 Pyruvate, 10 MgSO₄ 7H₂O, 0.5 CaCl₂ 2H₂O) and mounted in 0.3% LMP agarose (16520-100,
730 Life Technology). The lumbar spinal cords were sliced in a transverse plane (350 μm)
731 (VT1200S, Leica), and the spinal cord slices were recovered at 34°C for 30 minutes in
732 oxygenated (95% O₂ and 5% CO₂) HEPES holding solution (in mM: 86 NaCl, 2.5 KCl, 1.2
733 NaH₂PO₄, 35 NaHCO₃, 20 HEPES, 25 Glucose, 5 Sodium Ascorbate, 2 Thiourea, 3 Sodium
734 Pyruvate, 1 MgSO₄ 7H₂O, 2 CaCl₂ 2H₂O). After recovery, spinal cord slices were placed at RT
735 for 30 minutes prior to recordings. Spinal cord slices were then superfused with oxygenated
736 (95% O₂ and 5% CO₂) recording ACSF (in mM: 2.5 CaCl₂ 2H₂O, 1.0 NaH₂PO₄ H₂O, 119 NaCl,
737 2.5 KCl, 1.3 MgSO₄ 7H₂O, 26 NaHCO₃, 25 Glucose, 1.3 Sodium L-ascorbate) at RT in a
738 recording chamber mounted on a SliceScope Pro 6000 electrophysiology rig (Scientifica). Cells
739 were visualized by fluorescence to identify tdTomato positive cells, followed by infrared
740 differential interference contrast microscopy for patching (ORCA-Flash 4.0, Hamamatsu
741 Photonics; SliceScope Pro 6000, Scientifica). Whole-cell voltage-clamp recordings of
742 retrogradely labeled SPB neurons within superficial lamina were obtained under visual guidance
743 using a 40x objective. The Pipette resistance ranged from 3 to 4 MΩ, and the electrodes were
744 filled with an intracellular solution (in mM: 135 K-gluconate, 5 KCl, 0.5 CaCl₂, 5 EGTA, 5
745 HEPES, 5 MgATP, pH 7.2). Signals were acquired using a Multiclamp 700B amplifier
746 (Molecular Devices). The data were low-pass filtered at 2 kHz and digitized at 10 kHz with an
747 A/D converter (Digidata 1440A, Molecular Devices) and stored using a data acquisition program
748 (Clampex version 10, Molecular Devices). The liquid junction potential was not corrected.
749 Action potential (AP) discharges were recorded in current-clamp mode. For ChR2-assisted

750 circuit mapping, primary afferent synaptic terminals were stimulated with wide-field blue LED
751 illumination through the 40x objective (pE-300, CoolLED, 0.1 ms, 1 ms, and 10 ms pulse width,
752 light intensity = 27 mW). Cell capacitance, current amplitude, latency, and jitter were analyzed
753 using Clampfit (version 10, Molecular Devices). For pharmacology experiments, cells were
754 recorded in a solution containing 1 μ M tetrodotoxin (TTX) (1069, Tocris) followed by the
755 addition of 4-aminopyridine (4-AP; 500 μ M) (940, Tocris) to the bath.

756

757 **Tactile and thermal behavioral experiments.** Both male and female mice (2 - 6 months old) of
758 mixed genetic backgrounds were used for behavioral analyses (except for the real-time texture
759 aversion assay in which only male mice were used). All mice (experimental mice and littermate
760 controls) were group housed. Littermates from the same genetic crosses were used as controls for
761 each group to control for variability in mouse strains/genetic backgrounds. Experiments were
762 performed and analyzed by investigators who were blinded to genotype.

763 *von Frey test.* Mice were placed in clear plastic chambers on an elevated wire mesh and the
764 plantar surface of the hindpaw was stimulated with a set of calibrated von Frey filaments (North
765 Coast Medical) 10 times each (0.008 - 4 g). The number of paw withdrawal responses was
766 scored for each von Frey filament.

767 *Hot/cold plate.* Mice were placed on a 55°C hot plate or a 5°C cold plate (IITC) and their
768 behaviors were recorded using a camera (Hero 4, GoPro). Cut-off times were 20 seconds and 3
769 minutes for 55°C hot plate and 5°C cold plate, respectively. The number of paw-licking episodes
770 (hindpaw licking for hot plate and forepaw licking for cold plate) were manually scored by
771 analyzing video recordings.

772 *Real-time texture aversion.* Male mice were habituated in test chambers (black acrylic, 12 inches
773 x 11.8 inches x 6 inches, 0.25 inch-thickness) for 2 days (10 - 20 minutes each day) prior to the
774 test day. On the test day, mice were first placed in test chambers with a fresh sheet of dusty pink
775 construction paper (338293, Office Depot) on the floor and their baseline preference behaviors
776 were recorded for 10 minutes using a digital USB 2.0 CMOS video camera (60516, Stoelting)
777 mounted directly above the test chambers. Mice were then transferred to the test chambers with
778 sandpapers of two different textures (extra fine grit SP400 (smooth) and coarse grit SP150
779 (rough), McMaster-Carr) on the either side of the floor and their behaviors were recorded for 10

780 minutes. The mouse centroid was tracked, and the percentage of time spent on each side of the
781 test chamber was analyzed using a custom program written in Bonsai software (2.3.1)⁴¹.

782

783 **Optogenetic behavioral experiments.** The same criteria were used for mouse handling as
784 described above. Prior to experiments, fiberoptic cannulas implanted into the PBN_L were
785 attached through zirconia sleeves (Doric Lenses) to branching fiberoptic patchcords (Doric
786 Lenses) connected to a blue LED (Doric Lenses) and a programmable LED driver (Doric
787 Lenses). Optogenetic stimulation was controlled by the combination of custom programs written
788 in Bonsai software and Doric Neuroscience Studio (4.1.5.2) through an Arduino circuit board
789 (Uno, Arduino) and custom sketches written in Arduino software (1.8.7). Approximately the
790 initial half of the experiments were performed and analyzed by investigators who were not
791 blinded to genotype, and the remainder of the experiments were repeated by investigators who
792 were blinded to genotype.

793 *Locomotion and grooming analyses.* Mice were habituated in test chambers (Clear acrylic, 8.5
794 inches x 4.5 inches x 5.5 inches, 0.25 inch-thickness) for 2 days (20 minutes each day) prior to
795 the test day. On the test day, mice were placed in test chambers and photostimulation was
796 delivered as described in the figure legends. Locomotor and grooming behaviors were recorded
797 (30 frames/second) with two separate digital USB 2.0 CMOS video cameras mounted directly
798 above and in front of the test chambers. The mouse centroid was tracked, and speed and velocity
799 of mouse locomotion were analyzed at 2 Hz with video files filmed by the camera mounted
800 above of the test chambers using a custom program written in Bonsai software. Mouse grooming
801 and jumping behaviors were analyzed manually using video files filmed by the camera mounted
802 in front of the test chambers by investigators who were blinded to genotype.

803 *NBQX infusion.* 300 nl of either saline or the selective AMPA receptor antagonist NBQX (10
804 mM dissolved in saline, 1044, Tocris) was bilaterally infused into the PBN_L through fluid
805 injectors (Doric Lenses) inserted into the dual opto-fluid cannulas implanted into the PBN_L
806 (infusion rate was 100 nl / min). After the infusion, fluid injectors were swapped with optical
807 injectors (Doric Lenses) for photostimulation. Locomotor behavior was monitored 0.5 – 1.5
808 hours after the infusion.

809 *Pupilometry.* Mice were implanted with custom-cut headplates, which were then secured by
810 dental cement (Metabond, Parkell) application. After 3-5 days of recovery, mice were head-fixed

811 and acclimated on the custom-built behavioral apparatus for 2 days (20 - 30 minutes each day)
812 prior to the test day. On the test day, mice were head-fixed and acclimated on the behavioral
813 apparatus for 10 - 20 minutes, and a photostimulation was delivered as described in the figure
814 legends. Pupillary reactions were recorded (30 frames/second) using a digital USB 2.0 CMOS
815 video cameras mounted close to one eye. An infrared illuminator was used to obtain high
816 contrast images of the pupil. The pupil diameter was tracked at 10 Hz using a custom program
817 written in Bonsai software, and peak amplitude and area under the curve (AUC) were analyzed
818 using GraphPad Prism (Version 8, GraphPad Software). Relative change in pupil diameter
819 ($\Delta D/D$) was calculated as follows.

$$820 \quad \frac{\Delta D \text{ (pupil diameter} - \text{average baseline pupil diameter)}}{D \text{ (average baseline pupil diameter)}}$$

821 The average baseline pupil diameter was the average of pupil diameter during the one-minute
822 baseline period before the beginning of the first optogenetic stimulation. The long abrupt
823 downward lines in the raw traces of pupil diameter were used as a measure of the number of
824 blinks/squints.

825 *Real-time place preference.* Mice were habituated in test chambers (black acrylic, 12 inches x
826 11.8 inches x 6 inches, 0.25 inch-thickness) for 2 days (20 minutes each day) prior to the test
827 day. On the test day, mice were placed in test chambers and their preference behaviors during
828 pre-stimulation, stimulation, and post-stimulation sessions (10 minutes each session) were
829 recorded using a digital USB 2.0 CMOS video camera mounted directly above the test chambers.
830 The mouse centroid was tracked real-time using a custom program written in Bonsai software,
831 and photostimulation (10 Hz, 10 ms pulse width) was constantly delivered through Doric
832 Neuroscience Studio and Arduino coupled to the Bonsai program while mice stayed on one side
833 - “stimulated” side - of the chambers (counterbalanced between the two sides).

834 *Lever-pressing assay.* Two levers (ENV-110M, Med Associates) were placed side by side on one
835 side of the test chambers (black acrylic, 10 inches x 8 inches x 8 inches, 0.25 inch-thickness).
836 The original snap action switches inside of the levers were swapped with ones that have lower
837 operating force threshold (480-3021-ND, Digi-Key). The levers were calibrated using von Frey
838 filaments to operate following 4 - 6 g force application. Mice were habituated in test chambers
839 for 2 days (1 hour each day) prior to the test day, and the number of lever presses during the 1-
840 hour session on the third day was used as baseline. During the subsequent eight days (“light on”

841 sessions, 1-hour session each day), mice received an optogenetic stimulation (5 seconds, 10 Hz)
842 when they pressed the active lever, but not the inactive lever (counterbalanced between left and
843 right sides). The active lever was coupled to optogenetic stimulation through Doric Neuroscience
844 Studio and Arduino under control of a custom program written in Bonsai software. The
845 following 5 days (“light off” sessions, 1-hour session each day), optogenetic stimulation was
846 uncoupled from lever-pressing. The number of lever presses was recorded in real-time using
847 custom programs written in Arduino and Bonsai software.

848

849 **Statistical analysis.** Statistical analyses were performed using GraphPad Prism (Version 8,
850 GraphPad Software). The number of mice used and statistical analyses, including *post hoc*
851 multiple comparisons tests, used for individual experiments are indicated in the figure legends.
852 The following symbols were used in the figure legends for *p*-values: ns, not significant; *, $p <$
853 0.05; **, $p < 0.01$; ***, $p < 0.001$. The exact *p*-values can be found in the supplementary table 1.

854

855 **Reporting summary.** Further information on experimental design is available in the Nature
856 Research Reporting Summary linked to this paper.

857

858 **Data availability.** The data generated in this study are available from the corresponding author
859 upon reasonable request.

860

861 **Code availability.** The custom codes used in the study are available at GitHub
862 (<https://github.com/SebastianChoi/Choi-et-al-Nature2020>) or upon request.

863

864

- 865 31 Hooks, B. M., Lin, J. Y., Guo, C. & Svoboda, K. Dual-channel circuit mapping reveals
866 sensorimotor convergence in the primary motor cortex. *J Neurosci* **35**, 4418-4426,
867 doi:10.1523/JNEUROSCI.3741-14.2015 (2015).
- 868 32 Kim, J. C. *et al.* Linking genetically defined neurons to behavior through a broadly
869 applicable silencing allele. *Neuron* **63**, 305-315, doi:10.1016/j.neuron.2009.07.010
870 (2009).
- 871 33 Niederkofler, V. *et al.* Identification of Serotonergic Neuronal Modules that Affect
872 Aggressive Behavior. *Cell Rep* **17**, 1934-1949, doi:10.1016/j.celrep.2016.10.063 (2016).
- 873 34 Zhou, X. *et al.* Deletion of PIK3C3/Vps34 in sensory neurons causes rapid
874 neurodegeneration by disrupting the endosomal but not the autophagic pathway. *Proc*
875 *Natl Acad Sci U S A* **107**, 9424-9429, doi:10.1073/pnas.0914725107 (2010).

876 35 Rutlin, M. *et al.* The cellular and molecular basis of direction selectivity of Adelta-
877 LTMRs. *Cell* **159**, 1640-1651, doi:10.1016/j.cell.2014.11.038 (2014).
878 36 Vrontou, S., Wong, A. M., Rau, K. K., Koerber, H. R. & Anderson, D. J. Genetic
879 identification of C fibres that detect massage-like stroking of hairy skin in vivo. *Nature*
880 **493**, 669-673, doi:10.1038/nature11810 (2013).
881 37 Pivetta, C., Esposito, M. S., Sigrist, M. & Arber, S. Motor-circuit communication matrix
882 from spinal cord to brainstem neurons revealed by developmental origin. *Cell* **156**, 537-
883 548, doi:10.1016/j.cell.2013.12.014 (2014).
884 38 Fenno, L. E. *et al.* Targeting cells with single vectors using multiple-feature Boolean
885 logic. *Nat Methods* **11**, 763-772, doi:10.1038/nmeth.2996 (2014).
886 39 Tervo, D. G. *et al.* A Designer AAV Variant Permits Efficient Retrograde Access to
887 Projection Neurons. *Neuron* **92**, 372-382, doi:10.1016/j.neuron.2016.09.021 (2016).
888 40 Lin, J. Y., Knutsen, P. M., Muller, A., Kleinfeld, D. & Tsien, R. Y. ReaChR: a red-
889 shifted variant of channelrhodopsin enables deep transcranial optogenetic excitation. *Nat*
890 *Neurosci* **16**, 1499-1508, doi:10.1038/nn.3502 (2013).
891 41 Lopes, G. *et al.* Bonsai: an event-based framework for processing and controlling data
892 streams. *Front Neuroinform* **9**, 7, doi:10.3389/fninf.2015.00007 (2015).
893

894 **Acknowledgements**

895 We thank all members of the Ginty laboratory for discussions and critical feedback during the
896 course of the project. We thank David Paul and Clifford Woolf for feedback and critical
897 evaluation of the manuscript, Susan Dymecki for providing *Rosa26^{LSL-FSF-TeTx}* and *Rosa26^{FSF-LSL-}*
898 *SYN-GFP* mouse lines, LaTasha Crawford for help with initial characterization of the *Calca-FlpE*
899 BAC transgenic mouse line, Travis Dickendeshier for help with initial characterization of the
900 *Advillin^{FlpO}* knockin mouse line, Connie Cepko for providing AAV1-FLEX-PLAP viruses, Silvia
901 Arber for providing Cre-dependent AAV expression vector encoding synaptophysin-GFP, and
902 Caiying Guo and the Gene Targeting and Transgenic Facility at the Janelia Research Campus of
903 the Howard Hughes Medical Institute for generating mouse lines. We thank Bianca Kun, Maggie
904 Streeter, Celine Breton, and Olivia Gabriel for their assistance with mouse husbandry, and
905 histological and behavioral experiments. This work was supported by the Alice and Joseph E.
906 Brooks Funds (S.C.), the Blavatnik Biomedical Accelerator Fund (S.C. and D.D.G.), NIH grants
907 NS097344 and NS118454 (D.D.G.), NIH grant AR063772 (S.E.R.), NIH grant NS096705
908 (H.R.K.), NIH grant NS111643 (M.G.), the Bertarelli Foundation (D.D.G.), The Hock E. Tan
909 and Lisa Yang Center for Autism Research at Harvard Univeristy (D.D.G.), and the Edward R.
910 and Anne G. Lefler Center for Neurodegenerative Disorders (D.D.G). D.D.G. is an investigator
911 of the Howard Hughes Medical Institute.

912
913

914 **Author contributions**

915 S.C. and D.D.G. conceived and designed the project. S.C. screened and characterized the new
916 anterolateral pathway PN mouse lines, and designed, executed and analyzed the histology,
917 behavior, and spinal cord slice recording experiments. M.A.B., A.M. and N.I. assisted in
918 executing and analyzing histology and behavioral experiments. D.Z. assisted in RNAscope
919 analyses. M.M.D. and R.L.W. assisted in executing and analyzing behavioral experiments. The
920 *ex vivo* spinal cord physiological recordings were done by J.H., Y.O. and S.C, and analyzed by
921 J.H., Y.O., S.E.R., and H.R.K. N.H. and S.G. generated the *Calca-FlpE* BAC transgenic mouse

922 line. L.B. characterized *Calca-FlpE* and *Advillin^{FlpO}* mouse lines, and C.S. characterized
923 *Tau^{FSF^{iAP}}* mouse line. M.G. provided the *Lbx1^{FlpO}* mouse line. S.C. and D.D.G. wrote the
924 manuscript with input from all authors.

925

926 **Competing interests**

927 The authors declare no competing interests.

928 **Extended Data Figure Legends**

929

930 **Extended Data Figure 1. Generation of CreERT2 mouse lines for genetic labeling of**

931 **anterolateral pathway neurons and Flp mouse lines for labeling primary sensory neurons.**

932 **a1-a3**, Gene targeting strategies used to generate the *Robo3*^{IRES-CreERT2} (a1), *Tacr1*^{CreERT2} (a2),

933 and *Gpr83*^{CreERT2} (a3) mouse lines. **a1**, A 3X-STOP-IRES-CreERT2 cassette was introduced via

934 homologous recombination into the first common coding exon that is shared by different splice

935 variants of the *Robo3* gene. **a2**, A CreERT2 cassette was introduced via homologous

936 recombination into the *Tacr1* gene, replacing the first coding ATG. **a3**, A CreERT2 cassette was

937 introduced via homologous recombination into the *Gpr83* gene, replacing the first coding ATG.

938 IRES, internal ribosome entry site; s.int, synthetic intron; WPRE, Woodchuck Hepatitis Virus

939 (WHP) Posttranscriptional Regulatory Element; pA, poly A; f, FRT site; kz, kozak sequence. **b1-**

940 **b3**, A horizontal section of the lumbar spinal cord. 93.7 ± 2.6 % of tdTomato⁺ neurons were

941 *Tacr1*⁺, while 96.6 ± 2.4 % of *Tacr1*⁺ neurons were tdTomato⁺. n = 3 mice. **c**, A transverse

942 section of a *Gpr83*-GFP mouse. Green and red dots represent GFP and *Gpr83* mRNA molecules,

943 respectively, detected with gene-specific RNAscope probes. 96.0 ± 1.2 % of GFP⁺ cells were

944 *Gpr83*⁺, while 84.5 ± 5.0 % of *Gpr83*⁺ cells were GFP⁺. n = 2 mice. **d**, Distribution of tdTomato-

945 expressing *Robo3*⁺ neurons in the spinal cord dorsal horn (top) and their thalamic projections

946 terminating in the VPL (bottom). n = 2 mice. **e1-5**, Characterization of the *Advillin*^{FlpO} mouse

947 line. n = 4 mice. **e1-e3**, The *Advillin*^{FlpO} mouse line labels the majority of DRG neurons ($99.0 \pm$

948 0.1 % of NeuN⁺ neurons are tdTomato⁺) (e1), nodose ganglia neurons (80.8 ± 5.1 % of NeuN⁺

949 neurons are tdTomato⁺) (e2), and sympathetic ganglia neurons (98.6 ± 0.3 % of TH⁺ neurons are

950 tdTomato⁺) (e3). **e4**, A transverse section of the vertebral column. tdTomato⁺ Advillin-

951 expressing neurons and their axons are visualized in the spinal cord (asterisk), DRGs (arrows),

952 and sympathetic ganglia (arrowheads). **e5**, A coronal section of the brainstem. tdTomato⁺ axons

953 of Advillin-expressing neurons innervate the nucleus of the solitary tract (arrowhead), the dorsal

954 column nuclei (arrow), and the trigeminal nucleus (asterisk). **f1-4**, Characterization of the *Calca-*

955 *FlpE* mouse line. n = 2 mice. A cross section of the lumbar DRG (f1-f3) and a transverse section

956 of the lumbar spinal cord (f4). **f1-3**, 91.9 ± 1.5 % of tdTomato⁺ neurons were CGRP⁺, while 92.3

957 ± 1.5 % of CGRP⁺ neurons were tdTomato⁺. **f4**, tdTomato-expressing axons of CGRP⁺ DRG

958 neurons are CGRP immunoreactive in the spinal cord dorsal horn.

959
960 **Extended Data Figure 2. Comparative analysis of the *Gpr83*⁺, *Tacr1*⁺, and *Tacr1*⁺ SPB**
961 **populations. a**, Distribution of EYFP-expressing *Tacr1*⁺ (top) or *Gpr83*⁺ (bottom) spinal
962 neurons and mCherry-expressing *Gad2*⁺ neurons in the superficial lamina of the spinal cord
963 dorsal horn. **b**, Quantification of % of *Gad2*-negative neurons in EYFP⁺ neurons. 97.5 ± 1.4 % of
964 *Tacr1*⁺ neurons and 99.5 ± 0.5 % of *Gpr83*⁺ neurons were *Gad2*-negative. **c**, Distribution of
965 tdTomato-expressing *Tacr1*⁺ neurons and GFP-expressing *Gpr83*⁺ neurons in the spinal cord
966 dorsal horn. **d**, Quantification of co-expression of tdTomato and GFP. 80.2 ± 1.5 % and $87.0 \pm$
967 2.5 % of tdTomato-expressing *Tacr1*⁺ neurons are not positive for GFP expression in lamina
968 I+IIo and lamina IIid, respectively. Conversely, 78.0 ± 1.8 % and 92.0 ± 1.4 % of GFP-expressing
969 *Gpr83*⁺ neurons are not positive for tdTomato expression in lamina I+IIo and lamina IIid,
970 respectively. **e**, Distribution of EYFP-expressing *Tacr1*⁺ neurons, *Gpr83*⁺ neurons, or both in the
971 superficial lamina of the spinal cord dorsal horn. The SPB neurons were retrogradely labeled
972 with CTB injected into the PBN_L. Arrowheads, CTB and EYFP double-positive neurons. **f**,
973 Quantification for % of *Tacr1*⁺ SPB neurons, *Gpr83*⁺ SPB neurons, and either *Tacr1*⁺ or *Gpr83*⁺
974 SPB neurons. **g**, % of *Tacr1*⁺, *Gpr83*⁺, *Tacr1*⁺ *Gpr83*⁺, and *Tacr1*⁻ *Gpr83*⁻ SPB neurons
975 calculated from experiments in e, f. **h, i**, Coronal sections of the ventral brain stem of
976 *Tacr1*^{CreERT2} (f) or *Gpr83*^{CreERT2} (h) mice whose lumbar spinal cords were injected with AAV1-
977 FLEX-Synaptophysin-GFP viruses. MAO, medial accessory olivary nucleus; DAOdf, dorsal
978 accessory olivary nucleus dorsal fold; DAOvf, dorsal accessory olivary nucleus ventral fold; PO,
979 primary olivary nucleus. **j**, Distribution of tdTomato-expressing *Tacr1*⁺ neurons in the superficial
980 lamina of the spinal cord dorsal horn. The SPB neurons were retrogradely labeled with CTB
981 injected into the PBN_L. Arrowhead, CTB and tdTomato double-positive neuron. **k**,
982 Quantification of % of *Tacr1*⁺ SPB neurons. **l**, Schematic of injections of AAV2-retro-FlpO
983 viruses into the PBN_L. **m**, Distribution of tdTomato-expressing *Tacr1*⁺ (left) or *Gpr83*⁺ (right)
984 SPB neurons and *Tacr1*-expressing neurons in the spinal cord dorsal horn. tdTomato (red) and
985 *Tacr1* (green) mRNA molecules were detected with gene-specific RNAscope probes. Filled
986 arrowheads, double-positive neurons; empty arrowheads, tdTomato⁺ SPB neurons that do not
987 express *Tacr1*. **n**, Quantification of co-expression of tdTomato and *Tacr1* in lamina I+IIo. **o**,
988 Schematic of lumbar injections of an AAV1-FLEX-Synaptophysin-tdTomato virus. **p**,
989 Distribution of tdTomato-positive synaptic terminals of *Tacr1*⁺ SPB neurons in the PBN_L. **q**,

990 Quantification of distribution of tdTomato-positive synaptic terminals of *Tacr1*⁺ SPB neurons in
991 the PBN_L. n = number of mice (indicated in the graph). Error bars, s.e.m.

992

993 **Extended Data Figure 3. *Tacr1*⁺ and *Gpr83*⁺ spinal PNs that innervate the posterior**

994 **thalamus, midbrain, or the pons are distinct populations. a, d, g, Schematics of lumbar spinal**

995 **cord injections of AAV1-Con/F_{on}-EYFP viruses and brain injections of AAV2-retro-FlpO viruses**

996 **into the SCig of *Tacr1*^{CreERT2} mice (a) (n = 3 mice), the MGm/SPFp of *Tacr1*^{CreERT2} (d) (n = 2**

997 **mice) or *Gpr83*^{CreERT2} mice (g) (n = 3 mice). b, e, h, Transverse sections of cervical spinal cords**

998 **of *Tacr1*^{CreERT2} (b, e) or *Gpr83*^{CreERT2} mice (h). White dotted lines, tdTomato-expressing axons**

999 **traveling through spinal cord white matter. DLF, dorsal lateral funiculus; VLF, ventral lateral**

1000 **funiculus. c, f, i, Coronal sections of target brain regions of *Tacr1*⁺ (c, f) or *Gpr83*⁺ (i) spinal**

1001 **PNs. AQ, cerebral aqueduct.**

1002

1003 **Extended Data Figure 4. Strong axon terminal stimulation of *Tacr1*⁺ and *Gpr83*⁺ SPB**

1004 **neurons produces distinct locomotor behaviors. a, Association of synaptic terminals of *Tacr1*⁺**

1005 **and *Gpr83*⁺ SPB neurons with *Calca*-GFP-expressing cell bodies and neurites in the PBN_{EL}. b,**

1006 **Quantification of the number of synaptophysin-tdTomato puncta associated with GFP⁺ cell**

1007 **bodies and neurites. The numbers were normalized with the total GFP⁺ area (to normalize for the**

1008 **variability of total GFP⁺ area) and the total number of synaptophysin-tdTomato puncta within the**

1009 **entire PBN_L (to normalize for the variability of virus injections). AU, arbitrary unit. Two-tailed *t*-**

1010 **test; n = 4 mice each for *Tacr1*⁺ and *Gpr83*⁺ SPB neurons. c, Quantification of average speed**

1011 **during light-off periods following light-on periods (473 nm, 6.5 mW, 10 ms pulse width). One-**

1012 **way ANOVA (Dunnett's multiple comparisons test); $F_{[2, 16]} = 10.60$ (2 Hz), $F_{[2, 16]} = 40.12$ (5 Hz),**

1013 **$F_{[2, 16]} = 20.48$ (10 Hz). d, Average velocity of mice over time (6.5 mW, 2 Hz, 10 ms pulse**

1014 **width). Positive values indicate forward movement whereas negative values indicate backward**

1015 **movement. Shaded areas, s.e.m. e, f, Quantification of average velocity during light-on periods**

1016 **with 2 Hz (e) and 5 Hz (f) photostimulation. Note that mice receiving *Tacr1*⁺ SPB neuron**

1017 **terminal stimulation exhibited net negative velocity during the 2 Hz photostimulation and lack a**

1018 **velocity increase despite the dramatic increase in speed during 5 Hz photostimulation. Two-**

1019 **tailed *t*-test; n = 6, 5 mice for *Tacr1*, *Gpr83*, respectively. g, Distribution of Fos⁺ neurons in the**

1020 **spinal cord dorsal horn following either photostimulation of axon terminals of SPB neurons**

1021 (*Tacr1*⁺ or *Gpr83*⁺) or a capsaicin (0.1%) injection into a hindpaw. Photostimulation of axon
1022 terminals of SPB neurons did not induce significant Fos expression in the spinal cord, whereas a
1023 hindpaw injection of capsaicin induced strong Fos expression in the medial region of the
1024 superficial lamina of the spinal cord dorsal horn. d, dorsal; v, ventral, m, medial; l, lateral. n = 4,
1025 3, 5, 2 mice for control, *Gpr83*, *Tacr1*, Capsaicin, respectively. **h**, Quantification of the number
1026 of Fos⁺ neurons in lamina I and II. The number of Fos⁺ cells was quantified in the medial 200
1027 μm of the spinal cord dorsal horn. One-way ANOVA (Tukey's multiple comparisons test). Error
1028 bars, s.e.m.

1029

1030 **Extended Data Figure 5. Physiological response properties of *Tacr1*⁺ and *Gpr83*⁺ SPB**
1031 **neurons. a, b**, Summary violin plots of peak instantaneous firing rates of *Gpr83*⁺ (a) and *Tacr1*⁺
1032 (b) SPB neurons in response to von Frey indentations and thermal stimuli. Red lines indicate
1033 median, while blue lines indicate quartiles. Friedman test (Dunn's multiple comparison test). n =
1034 16, 15 neurons for *Tacr1*⁺, *Gpr83*⁺, respectively. **c**, Representative traces of action potential
1035 firing evoked by topical capsaicin (0.05%) treatment. Arrows, time when capsaicin was applied
1036 to the skin. **d**, Quantification of peak instantaneous firing rates upon capsaicin application.
1037 Mann-Whitney test (two-tailed); *p* value is indicated; n = 11, 7 neurons for *Tacr1*⁺, *Gpr83*⁺,
1038 respectively; error bars, s.e.m.

1039

1040 **Extended Data Figure 6. Simultaneous inhibition of the synaptic outputs of both *Tacr1*⁺**
1041 **and *Gpr83*⁺ SPB neurons attenuates nocifensive behaviors in response to noxious cutaneous**
1042 **stimuli. a**, Hindpaw-licking was scored while *Tacr1*^{CreERT2}; *Lbx1*^{FlpO}; *Rosa26*^{LSL-FSF-TeTx} mice,
1043 *Gpr83*^{CreERT2}; *Lbx1*^{FlpO}; *Rosa26*^{LSL-FSF-TeTx} mice, or *Tacr1*^{CreERT2}; *Gpr83*^{CreERT2}; *Lbx1*^{FlpO};
1044 *Rosa26*^{LSL-FSF-TeTx} mice were placed on the 55°C hot plate (cut-off time, 20 seconds). These
1045 intersectional strategies target the entire *Tacr1*⁺ and *Gpr83*⁺ spinal populations, of which 34.2%
1046 (20.5% PBN_L-projecting, 6.6% PAG-projecting, and 7.1% MGm/SPFp-projecting PNs are
1047 combined) and 30.9% (14.0% PBN_L-projecting, 4.6% PAG-projecting, and 12.3% MGm/SPFp-
1048 projecting PNs are combined) are *Tacr1*⁺ and *Gpr83*⁺ PNs (laminal/IIo and the LSN are
1049 combined), respectively (a detailed description of the quantification is in the methods). Two-
1050 tailed *t*-test. **b**, Forepaw-licking was scored while mice were placed on the 5°C cold plate (cut-
1051 off time, 3 minutes). Two-tailed *t*-test. **c**, Paw withdrawal frequency following hindpaw skin

1052 indentation using von Frey filaments was scored. Two-way ANOVA; p value is indicated; $F_{[1, 43]}$
1053 = 8.65 for *Tacr1*/*Gpr83*-TeTx. **d**, Real-time texture aversion assay (150 grit sand paper vs 400
1054 grit sand paper). % of time spent in rough side of sand paper (150 grit) was measured
1055 (normalized to baseline preference). Two-tailed t -test. **e, f**, The suppression of neurotransmission
1056 in the quadruple transgenic mice was confirmed by reduced Fos induction in the PBN_L following
1057 exposure of mice to noxious thermal stimuli. **e**, Distribution of Fos⁺ neurons in the PBN_L
1058 following thermal stimulation. **f**, Quantification of the number of Fos⁺ neurons in the PBN_L.
1059 One-way ANOVA (Tukey's multiple comparisons test); $F_{[2, 9]} = 8.97$ (5°C), $F_{[2, 8]} = 27.09$
1060 (55°C). n = number of mice (indicated in the graphs). Error bars, s.e.m.

1061
1062 **Extended Data Figure 7. *Gpr83*⁺ and *Tacr1*⁺ SPB neurons receive strong synaptic inputs**
1063 **from *Mrgprd*⁺ polymodal non-peptidergic sensory neurons and weak, sparse, and**
1064 **polysynaptic inputs from distinct primary sensory neurons, and exhibit distinct dendritic**
1065 **morphologies. **a****, Distribution of CGRP⁺, *Mrgprb4*⁺, *Mrgprd*⁺, and *Ntrk2*⁺ primary afferent
1066 synaptic terminals in the spinal cord dorsal horn. The *Rosa26^{FSF-LSL-SYN-GFP}* reporter mouse line³³
1067 was used in combination with sensory neuron Cre/FlpE mouse lines and *Advillin^{FlpO}/Advillin^{Cre}*
1068 mouse lines. Note that CGRP⁺, *Mrgprb4*⁺, *Mrgprd*⁺, and *Ntrk2*⁺ primary afferent synaptic
1069 terminals mainly innervate lamina I+IIo, IIid, IIid, and IIiv+III, respectively. **b-d**,
1070 Quantifications of peak current density in *Tacr1*⁺ (c, d) and *Gpr83*⁺ (b) SPB neurons elicited by
1071 long light pulse-stimulation (1 ms and 10 ms) of CGRP⁺ (b), *Mrgprb4*⁺ (c), and *Ntrk2*⁺ (d)
1072 primary afferent terminals. The same neurons, stimulated with different durations of light
1073 stimulation, are connected by dotted lines. Note that only a small fraction of *Gpr83*⁺ SPB
1074 neurons exhibited long-latency (21.68 ± 2.66 ms), high-jitter (2.97 ± 0.85 ms) polysynaptic
1075 EPSCs with 10 ms-long photostimulation of CGRP⁺ afferent terminals and, conversely, only a
1076 small fraction of *Tacr1*⁺ SPB neurons exhibited long-latency (14.29 ± 3.49 ms), high-jitter (4.31
1077 ± 2.31 ms) polysynaptic EPSCs with 10 ms-long photostimulation of *Mrgprb4*⁺ afferent
1078 terminals. 2 out of 7 *Tacr1*⁺ SPB neurons exhibited long-latency (11.89 ± 4.18 ms), but relatively
1079 low-jitter (0.57 ± 0.21 ms) synaptic EPSCs following 10 ms-long photostimulation of *Ntrk2*⁺
1080 afferent terminals. **e**, Representative traces of light-activated currents (left) and AP firing (right)
1081 upon photostimulation of *Mrgprd*⁺ primary afferent terminals. Turquoise bars, 0.1 ms (EPSCs)
1082 and 1 ms (APs) LED (473 nm) stimulations. **f**, Quantifications of peak current density. Mann-

1083 Whitney test (two-tailed); n = number of neurons. **g**, Schematic of injections of AAV2-retro-
1084 FlpO viruses into the PBN_L. **h**, Distribution of tdTomato-expressing dendrites of *Tacr1*⁺ (top)
1085 and *Gpr83*⁺ (bottom) SPB neurons. Lamina II_{id} is labeled using IB4 binding. Arrowheads,
1086 *Gpr83*⁺ dendrites that are extended into deeper lamina of the spinal cord dorsal horn. **i**,
1087 Quantification of distance between the cell bodies and the outer boundary of IB4⁺ lamina II_{id}
1088 (dotted line). #, note that a small number of *Gpr83*⁺ SPB neurons have their cell bodies located
1089 within lamina II_{id}. n = 65, 60 neurons for *Tacr1*⁺, *Gpr83*⁺, respectively. **j**, **k**, Quantifications of
1090 total length of dendrites in a spinal cord section image within (j) or below (k) IB4⁺ lamina II_{id}
1091 (normalized to the total length of the IB4⁺ lamina II_{id} in the same spinal cord section image).
1092 Two-tailed *t*-test; n = 18, 23 sections (40 μm) for *Tacr1*⁺, *Gpr83*⁺, respectively. Error bars, s.e.m.

1093

1094 **Extended Data Figure 8. Anatomical analyses of axonal projections of anterolateral**

1095 **pathway PNs innervating the PBN_L and the inferior olivary complex.** **a**, Schematic of dual-

1096 CTB injections into the PBN_L. **b**, Distribution of CTB-labeled neurons in the spinal cord lamina

1097 I+II_o and the LSN. **c**, Quantification of % of SPB neurons that innervate the PBN_L

1098 contralaterally, ipsilaterally, or bilaterally. n = 3 mice. Error bars, s.e.m.

1099 **d**, Bottom view of a single axon trace of sparsely labeled *Gpr83*⁺ spinal PN that innervate the

1100 inferior olivary complex. Arrowhead, an axon branch traveling up to the rostral brain. r, rostral;

1101 c, caudal, m, medial; l, lateral. **e**, Quantification of the number of inferior olivary complex-

1102 projecting spinal PNs that exhibit dedicated vs. collateral-forming axons. **f**, Synaptic terminals of

1103 *Tacr1*⁺ (h) or *Gpr83*⁺ (i) PNs representing hindlimb regions (GFP) and forelimb regions

1104 (tdTomato), are segregated in the inferior olivary complex. n = 3 mice each for *Tacr1*⁺ and

1105 *Gpr83*⁺ PNs.

1106

1107 **Extended Data Figure 9. Photostimulation of either *Tacr1*⁺ or *Gpr83*⁺ SPB neuron axon**

1108 **terminals promotes rostral grooming, and produces distinct behaviors in instrumental**

1109 **conditioning assays.** **a**, Duration of rostral grooming of control (black line), *Gpr83*^{CreERT2};

1110 *Lbx1*^{FlpO}; *Rosa26*^{LSL-FSF-ReaChR} (green line), or *Tacr1*^{CreERT2}; *Lbx1*^{FlpO}; *Rosa26*^{LSL-FSF-ReaChR} (red

1111 line) mice over time. Bin size, 30 seconds. Axon terminals in the PBN_L were stimulated with

1112 blue LED (473 nm, 1 mW, 10 Hz, 10 ms pulse width) for 30 seconds 4 times (1 minute light-off

1113 periods between photostimulation periods). **b**, Quantification of average duration of rostral

1114 grooming during light-on periods for 0.4 mW, 1 mW, and 6.5 mW photostimulation. One-way
1115 ANOVA (Dunnett's multiple comparisons test); $F_{[2, 18]} = 7.60$ (1 mW), $F_{[2, 16]} = 7.49$ (6.5 mW); n
1116 = 6, 6, 9 mice (0.4 mW), 6, 7, 9 mice (1 mW), 8, 5, 6 mice (6.5 mW) for control, Gpr83, Tacr1,
1117 respectively. **c**, Schematic of lumbar injections of AAV1-hSyn-FlpO viruses. **d**, Quantification
1118 of total duration of grooming of different body parts during light-on periods. Axon terminals in
1119 the PBN_L were stimulated with blue LED (473 nm, 10 mW, 5 or 10 Hz, 10 ms pulse width) 4
1120 times for 1 minute each (1 minute light-off periods between photostimulation periods). $n = 4$
1121 trials (2 mice; 2 trials per mouse, 5Hz and 10 Hz stimulation) for *Tacr1*⁺ SPB neuron terminal
1122 stimulation, $n = 6$ trials (3 mice; 2 trials per mouse, 5Hz and 10 Hz stimulation) for *Gpr83*⁺ SPB
1123 neuron terminal stimulation. Paired *t*-test (two-tailed). **e**, Weak self-administered
1124 photostimulation (0.4 mW) of *Gpr83*⁺ SPB neuron terminals led to an increase in the number of
1125 presses for the active lever, but not the inactive lever over time. **f**, Self-administered
1126 photostimulation (1 mW) of *Tacr1*⁺ SPB neurons led to a decrease in the number of presses for
1127 the active lever, but not inactive lever over time. Turquoise boxes indicate 8 days of light-on
1128 sessions. $n = 7$ mice (Gpr83, 0.4 mW; Tacr1, 1 mW). Two-way repeated measures ANOVA; $F_{[1, 6]} = 8.23$
1129 (Gpr83, 0.4 mW), $F_{[1, 6]} = 9.43$ (Tacr1, 1 mW). Error bars, s.e.m.

1130

1131 **Extended Data Figure 10. Summary of two parallel ascending SPB pathways and a**
1132 **phylogenetic tree of structurally-related GPCR family proteins. a**, Summary cartoon of two
1133 parallel ascending SPB pathways for affective touch and pain. **b**, A phylogenetic tree generated
1134 using a multiple sequence alignment algorithm, ClustalW2 (EMBL-EBI). The top 14 mouse
1135 proteins that have the highest amino acid sequence similarity to mouse GPR83 were used for this
1136 analysis.

1137

1138

1139

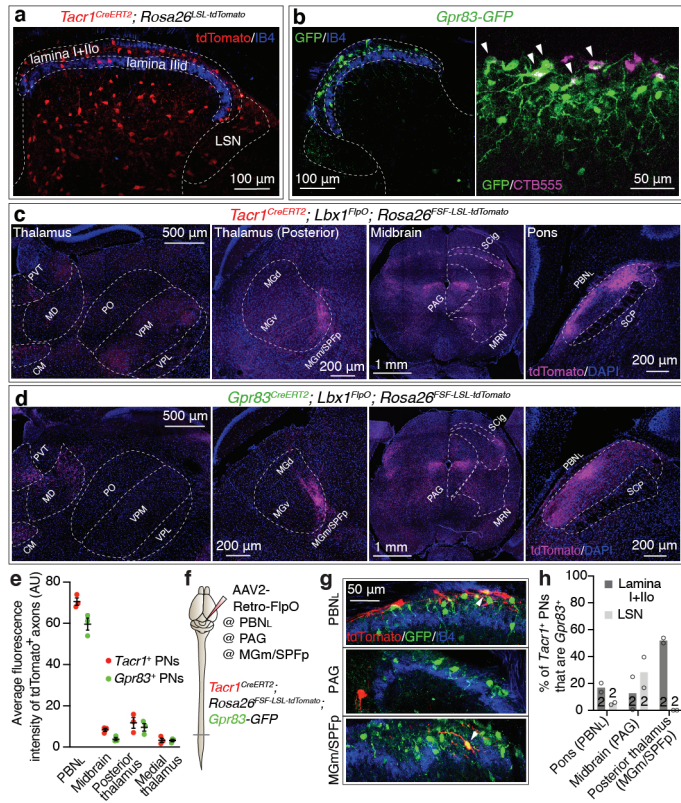


Figure 1

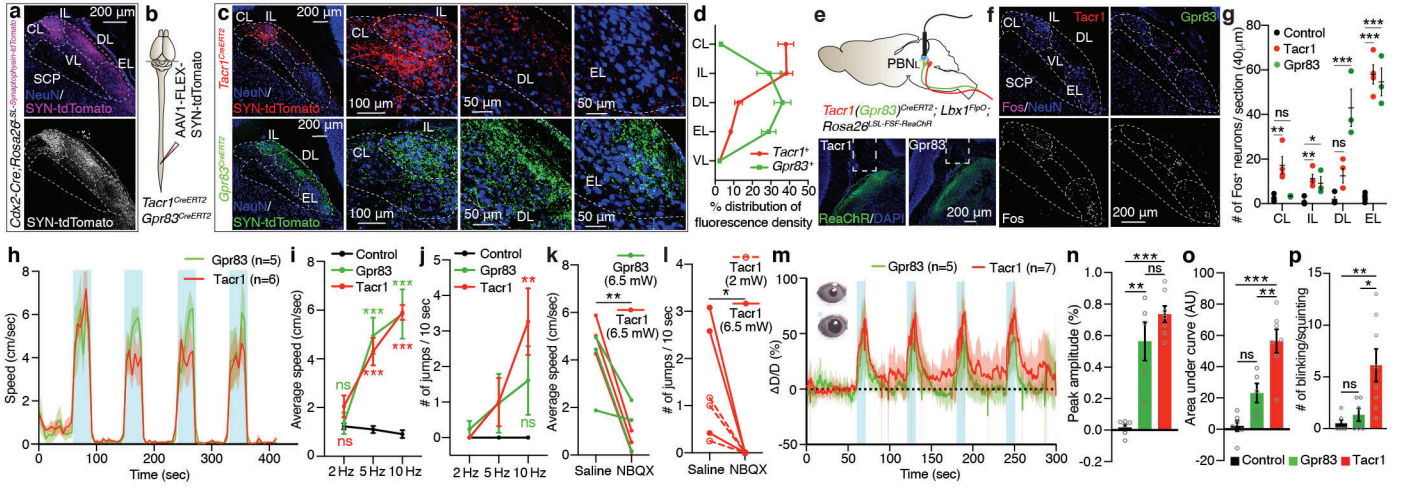


Figure 2

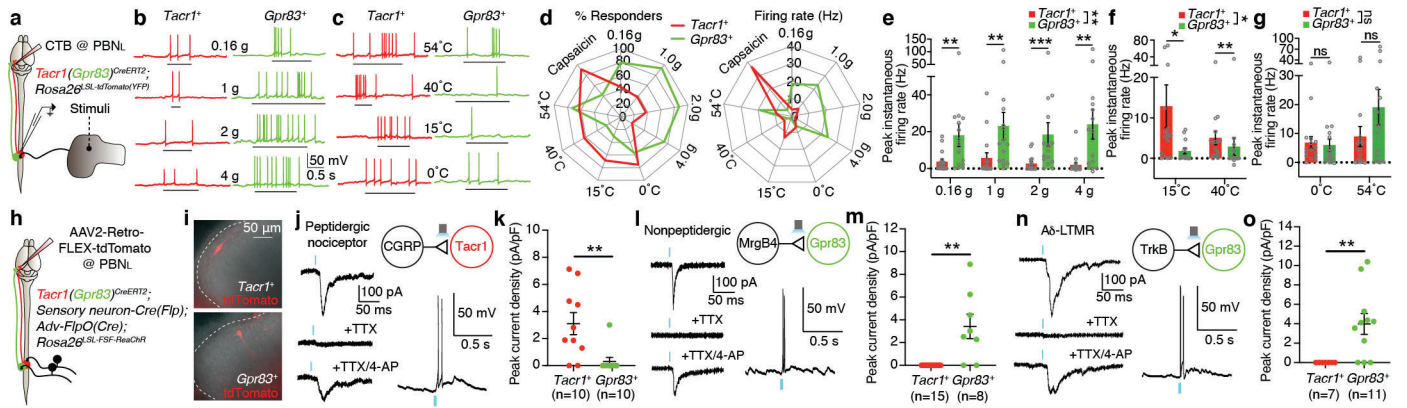


Figure 3

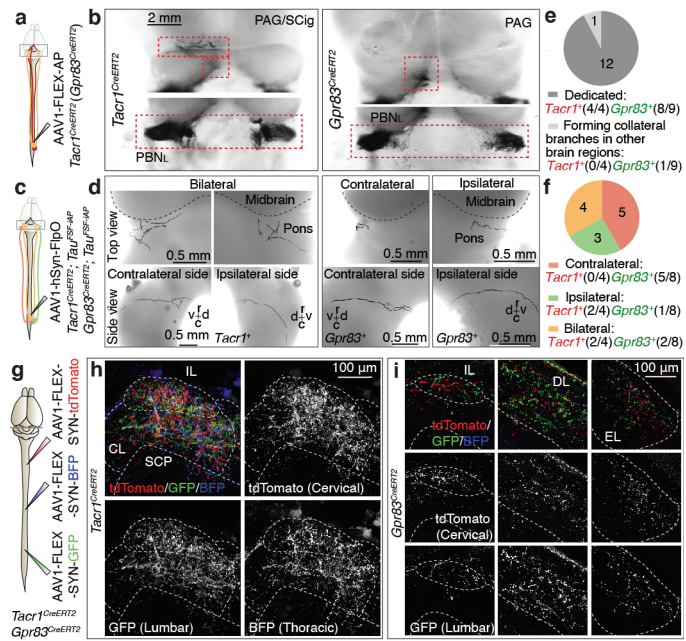


Figure 4

